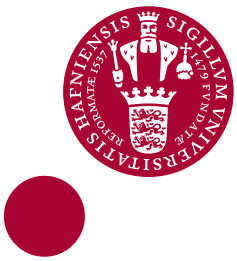

Isotope record of mineralogical changes in a spectrum of aqueously altered CM chondrites

van Kooten, Elishevah M. M. E.; Cavalcante, Larissa L.; Nagashima, Kazuhide; Kasama, Takeshi; Balogh, Zoltan, I; Peeters, Zan; Hsiao, Silver Sung-Yun; Shang, Hsien; Lee, Der-Chuen; Lee, Typhoon; Krot, Alexander N.; Bizzarro, Martin

Published in:
Geochimica et Cosmochimica Acta

DOI:
10.1016/j.gca.2018.06.021

Publication date:
2018

Document version
Publisher's PDF, also known as Version of record

Available online at www.sciencedirect.com

ScienceDirect

Geochimica et Cosmochimica Acta 237 (2018) 79–102

Geochimica et Cosmochimica Acta

www.elsevier.com/locate/gca

Isotope record of mineralogical changes in a spectrum of aqueously altered CM chondrites

Elishevah M.M.E. van Kooten [a,*], Larissa L. Cavalcante [a,b], Kazuhide Nagashima [c], Takeshi Kasama [d], Zoltan I. Balogh [d], Zan Peeters [e], Silver Sung-Yun Hsiao [e,f], Hsien Shang [e,f], Der-Chuen Lee [e,f], Typhoon Lee [e,f], Alexander N. Krot [a,c], Martin Bizzarro [a]

[a] *Centre for Star and Planet Formation and Natural History Museum of Denmark, University of Copenhagen, DK-1350 Copenhagen, Denmark*
[b] *Institute of Chemistry, University of São Paulo, 03178 São Paulo, Brazil*
[c] *Hawai'i Institute of Geophysics and Planetology, University of Hawai'i at Manoa, HI 96822, USA*
[d] *Centre for Electron Nanoscopy, Technical University of Denmark, DK-2800 Copenhagen, Denmark*
[e] *Institute of Astronomy and Astrophysics, Academia Sinica, P.O. Box 23-141, Taipei 10617, Taiwan, ROC*
[f] *Institute of Earth Science, Academia Sinica, 11529 Tapei, Taiwan*

Received 8 August 2017; accepted in revised form 15 June 2018; available online 25 June 2018

Abstract

The recent fall of the relatively unaltered CM chondrite Maribo provides a unique opportunity to study the early stages of aqueous alteration on the CM chondrite parent body. We show using transmission electron microscopy of a matrix FIB-section from Maribo that this meteorite mainly appears to consist of tochilinite-cronstedtite intergrowths (TCIs), but also contains regions of amorphous or nanocrystalline silicates, anhydrous silicates and FeNi metal aggregates with thin iron oxide rims, suggesting that it experienced aqueous alteration to a relatively small degree. A comparison of Maribo with increasingly altered CM chondrites such as Jbilet Winselwan and Bells shows that during progressive aqueous alteration (1) the TCIs are replaced by coarser sulfides and increasingly Mg-rich serpentine, and (2) the abundance of ^{15}N-rich hotspots increases, whereas the magnitude of their ^{15}N enrichment decreases. We observe that the overall N isotope variability related to aqueous alteration is an order of magnitude lower than the variability observed between different chondrite groups. We suggest these high order differences are the result of heterogeneous accretion of insoluble or soluble organic carriers of ^{15}N to the different chondrite parent bodies. D/H ratios of matrices from Maribo, Jbilet Winselwan and Bells increase with progressive aqueous alteration, a trend that is opposite to expectations of mixing between D-poor water and D-rich organic matter. We argue that this behaviour cannot be related to Fe oxidation or serpentinization reactions and subsequent loss of D-poor H_2 gas. We offer an alternative hypothesis and suggest that CM chondrites experienced two-stage aqueous alteration. During the first stage occurring at relatively low temperature, mixing of increasing amounts of D-poor water with D-rich organic matter results in a decrease of D/H ratio with increasing degree of alteration. During the second stage of alteration occurring at relatively high temperature ($T < 300$ °C), decomposition of TCIs in CMs of petrologic type <2.7 releases gaseous D-poor water that results in increase of the D/H ratio of the CM matrices. Finally, we report on changes in the organic structure of Maribo, Jbilet Winselwan and Bells using Carbon-K and Nitrogen-K edge electron energy loss spectroscopy. The organic matter initially has higher aromatic/aliphatic ratios (e.g., Maribo) and lower abundances of ketone and carboxyl functional groups, which we suggest are the result of chemical degradation of double bonded carbon from oxidation during hydrothermal

* Corresponding author.
E-mail address: elishevah.vankooten@snm.ku.dk (E.M.M.E. van Kooten).

https://doi.org/10.1016/j.gca.2018.06.021

alteration. Consequently, we propose that the organic matter of the CM chondrite Paris, for which lower aromatic/aliphatic ratios have been observed, may have been different from Maribo, perhaps reflecting the early accretion of Paris relative to Maribo.

Keywords: CM chondrites; Aqueous alteration; Maribo

1. INTRODUCTION

Carbonaceous chondrites are fragments of hydrated asteroids that likely represent left-over building blocks of the outer Solar System, beyond the accretion region of Jupiter (Van Kooten et al., 2016; Olsen et al., 2016; Budde et al., 2016). These meteorites are among the oldest and most primitive objects that provide insights into the early protoplanetary disk and the formation and dynamics of the planets (Scott, 2007). However, most carbonaceous chondrites are altered to various degrees, either through aqueous alteration or thermal metamorphism on their parent bodies (Krot et al., 2003). Hence, it is considered high priority to track the evolution of chondrite parent bodies after they accreted in order to understand the initial conditions of asteroid and planet formation.

CM (Mighei-like) chondrites are the most common group of carbonaceous chondrites and are also ubiquitously present as clasts within other meteorite groups (Zolensky et al., 1996), suggesting they are derived from one or more asteroids that dominated the accretion region of carbonaceous chondrites. Moreover, CM chondrites are represented by a wide petrological range (from weakly altered [2.9] to fully altered [2.0]) corresponding to various degrees of aqueous alteration (Rubin et al., 2007). Recent CM chondrite acquisitions of the Paris (find, unknown location, 2001) and Maribo (fall, Denmark, 2009) meteorites add to this range by representing the most unaltered CM chondrites to date (petrological type > 2.8, Zanda et al., 2010; Haack et al., 2012; Hewins et al., 2014). This makes CM chondrites unique samples to study the complete spectrum of aqueous alteration.

Several attempts have been made to classify CM chondrites by degree of aqueous alteration using mineralogical, compositional and isotopic indicators (Tomeoka and Buseck, 1985; Tomeoka et al., 1989; Browning et al., 1996; Lauretta et al., 2000; Rubin et al., 2007; Chizmadia and Brearley, 2008; Howard et al., 2009, 2011; Alexander et al., 2013). Most notably, previous studies focused on decomposition of CM chondrites' most typical constituents, the tochilinite-cronstedtite intergrowths (TCIs). These TCIs are also known as Poorly/Partially Characterized Phases (PCPs), depending on grain size for classification purposes (we use either term where appropriate throughout the paper). The conversion from tochilinite (an interlayering of sulfide and brucite) to sulfides, and cronstedtite (Fe-rich serpentine) to more Mg-rich serpentine is characterized by decreasing S/SiO_2 and FeO/SiO_2 ratios in PCPs and is used most commonly as the scale of progressive aqueous alteration in CM chondrites (Rubin et al., 2007). In the same study, Rubin et al. (2007) use a composite index of chondrule alteration, carbonate complexity and metal abundance among others to define the scale of alteration between moderately (type 2.6) and severely altered (type 2.0) CM chondrites. Mineralogical and chemical scaling of alteration were more recently complemented by stable isotope investigations of N, C and H in CM chondrites (Alexander et al., 2013), suggesting decreasing D/H and $^{15}N/^{14}N$ ratios with increasing aqueous alteration on a bulk scale (i.e., multiple grams of meteorite). That the alteration scales from Rubin et al. (2007) and Alexander et al. (2013) are complementary is emphasized further by the bulk D/H ratio of Paris ($D/H = 174.5 \times 10^{-6}$, Vacher et al., 2016 and Erratum), which falls on a correlation line between bulk D/H ratios and petrological type as determined by Rubin et al. (2007) and Alexander et al. (2013). However, bulk stable isotope measurements contribute little to understand the detailed processes of alteration on a smaller scale. For example, H isotope analyses of individual chondritic components such as the matrix can help understand progressive aqueous alteration and define the H-bearing precursors. Piani et al. (2018) used in situ H isotope analyses of CM chondrite matrices and suggested different origins for the water composition of Paris versus other CM chondrites. In addition, Sutton et al. (2017) demonstrate *increasing* D/H ratios of bulk CMs – as opposed to reported decreasing D/H (Alexander et al., 2012) – with progressive aqueous alteration, which they suggest are the result of Fe oxidation reactions in chondrites. Hence, more detailed H isotope investigations of CM chondrites could highlight sources of water ices and chemical processes during alteration, such as oxidation of Fe, organics and hydration of silicates, whereas small scale N isotope analyses could shed light on the contribution of different ^{15}N carriers from IOM (insoluble) and SOM (soluble organic matter) to the hydration process.

Complex organic matter observed in chondrites is subject to structural and compositional changes during aqueous alteration and/or thermal metamorphism (Pizzarello et al., 2006). It is important to characterize these changes to understand the formation of prebiotic molecules from the molecular cloud and protoplanetary disk stage to their incorporation in meteorites. While organic matter in the CM2.5 chondrite Murchison is studied extensively (Cronin and Chang, 1993; Cody and Alexander, 2005; Pizzarello et al., 2006; Derenne and Robert, 2010; LeGuillou et al., 2014), only recently a comparison was made between this chondrite and the weakly altered CM2.8 Paris (Vinogradoff et al., 2017). Collectively, these results suggest that hydrothermal alteration on the CM parent body induced aromatization and oxidation of the IOM.

To test the significance of these findings, a comparative study of the molecular structures from another set of CM chondrites is necessary.

The recent fall of Maribo, a CM chondrite characterized as 'highly unaltered' (Haack et al., 2012), provides a unique opportunity to study the early stages of aqueous alteration on the CM chondrite parent body. Here, we investigate the matrix mineralogy of Maribo by transmission electron microscopy (TEM), the H, N and C isotope composition of the matrix by secondary ion mass spectrometry (SIMS) and the structure of organic matter by electron energy loss spectroscopy (EELS). We use the same techniques on the moderately altered CM chondrite Jbilet Winselwan (type 2.0–2.7, Pernet-Fisher et al., 2009; Russell et al., 2014; Bischoff et al., 2017) and the heavily altered anomalous CM chondrite Bells (type ~2.1, Rubin et al., 2007) for comparison. Since our study does not contain a typical CM2.0 chondrite, we report mainly on isotopic and mineralogical changes occurring during the first stages of aqueous alteration. Our main results show (1) varying H isotope behaviour for different stages of CM chondrite alteration (2) N isotope variability in CM chondrites related to aqueous alteration is an order of magnitude smaller than variability related heterogeneous accretion of ^{15}N carriers and (3) we observe increasing oxidation of organic matter with an initially high aromatic/aliphatic ratio.

2. MATERIALS AND METHODS

2.1. Materials

We selected three CM chondrites with aqueous alteration degrees increasing from Maribo, Jbilet Winselwan and Bells (the fall, Alexander et al., 2012) based on classification schemes using PCP compositions (Rubin et al., 2007) and bulk oxygen isotope signatures (Clayton and Mayeda, 1999). Maribo is a recent fall and considered to be one of the least altered CM chondrites, with an alteration degree similar to the Paris meteorite (Zanda et al., 2010; Haack et al., 2012; Hewins et al., 2014). Bulk oxygen isotope data of Maribo ($\delta^{17}O = -1.27‰$; $\delta^{18}O = 4.96‰$; $\Delta^{17}O = -3.85‰$; Haack et al., 2012) are similar to Paris ($\delta^{17}O = -1.37‰$; $\delta^{18}O = 3.34‰$; $\Delta^{17}O = -3.11‰$) and consistent with a low degree of alteration (Clayton and Mayeda, 1999). Furthermore, PCP compositions of Maribo ($S/SiO_2 = 0.69$, $FeO/SiO_2 = 4.56$; Haack et al., 2012) according to the classification scheme by Rubin et al. (2007) show that Maribo, although containing altered phases, has a petrological type > 2.8. This is confirmed by detailed investigations of the TCI structures in Maribo (Vollmer et al., 2014). Unlike Maribo, Jbilet Winselwan is a heavily brecciated CM chondrite that contains clasts with petrological types ranging between 2.0 and 2.6 (Pernet-Fisher et al., 2009; Bischoff et al., 2017) and with some clasts that are even less altered (petrological type 2.7, Russell et al., 2014). Jbilet Winselwan is suggested to represent a C-type asteroid regolith with various lithologies, some of them showing signs of impact heating (Zolensky et al., 2016). Bells is considered an anomalous brecciated CM chondrite. Its bulk oxygen isotope composition (Rowe et al., 1994), noble gas signatures (Zadnik, 1985) and chemical composition (Mittlefehldt, 2002) indicate that Bells is a CM chondrite, but the matrix mineralogy – including saponite-rich phyllosilicates and a high abundance of magnetite – has closer affinities to CI chondrites. Moreover, Bells' insoluble organic matter (IOM) is extremely enriched in $^{15}N/^{14}N$ and D/H relative to other CM chondrites. Bells is classified by Rubin et al. (2007) as 2.1, whereas Browning et al. (1996) suggest that Bells is in fact a weakly altered CM chondrite, similar to Murchison (CM2.5). Besides looking at Maribo and Jbilet Winselwan to identify mineralogical, isotopic and structural changes during the earliest stages of alteration, we chose Bells to determine whether this anomalous chondrite accreted to the CM chondrite parent body or belongs to a different parent body.

2.2. Electron microprobe measurements

From each sample, a 1 × 1 cm section was polished and backscattered electron (BSE) images of the entire section were made on the UH JEOL JXA-8500F field-emission electron microprobe (Hawai'i). The chemical compositions of chondrule rims, intra-chondrule matrix regions (i.e., dust components that cannot be defined as chondrule rims) and PCPs were analyzed using a 5 nA focused beam with a 10 μm beam size (see Electronic Annex for further analytical conditions). Cronstedtite and tochilinite interlayering in PCPs from Jbilet Winselwan are typically smaller than the beam size and thus prevented single layer analysis. We therefore measured bulk PCP grains in close vicinity to the analyzed matrix sections from Jbilet Winselwan (small circles in Fig. 2) and averaged the FeO/SiO_2 and S/SiO_2 ratios to obtain the PCP composition of a particular region. Since cronstedtite and tochilinite grains are separated in Maribo, we applied the same method used by Haack et al. (2012) by taking a 1:1 ratio of these minerals.

2.3. N, C and H isotope measurements

Nitrogen, carbon and hydrogen isotopes were measured with the UH Cameca ims-1280 ion microprobe following protocols detailed in van Kooten et al. (2017). Secondary ion images of H^-, $^{12}C^-$, $^{13}C^-$, $^{18}O^-$, $^{12}C^{14}N^-$, $^{12}C^{15}N^-$ and $^{28}Si^-$ from 50 × 50 μm rastered areas were collected sequentially on the axial electron multiplier with mass resolving power of ~6500. Carbon and nitrogen isotope ratios from chondrule dust rims and intra-chondrule matrix areas of the CM chondrites were calculated from $^{13}C^-/^{12}C^-$ and $^{12}C^{15}N^-/^{12}C^{14}N^-$, respectively. To correct for instrumental mass fractionation (IMF), the Orgueil CI chondrite was used as a reference standard and measured before analysis of unknowns. In close proximity of these rasters, we analyzed the bulk H isotope composition of the phyllosilicates in 25 × 25 μm rasters, using an O^- primary beam. Two end members of the serpentine group (antigorite: $[Mg, Fe^{2+}]_3Si_2O_5[OH]_4$ and chrysotile: $Mg_3SiO_5[OH]_4$; Alt and Shanks, 2015) were chosen as standards to be measured in between sample runs to correct for IMF. N, C and H isotope ratios are presented in the delta notation after dead time (L'image, L. Nittler, DTM, Carnegie Inst.

Washington), time interpolation (Coakley et al., 2005) and IMF corrections (see Electronic Annex for details).

2.4. Stem-EELS

We selected a total of four ^{15}N-rich domains in Bells, Jbilet and Maribo for extraction by focused ion beam (FIB) in-situ lift-out with an FEI Helios SEM, equipped with an EDAX SD Apollo 10 Pegasus EDS and an Omniprobe manipulator at DTU-Cen in Copenhagen according to methods described in van Kooten et al. (2017). The selection of ^{15}N-rich domains is based on their extractability from the sample, rather than petrological setting in the CM chondrite sections. As outlined below, domains are taken from both intra-chondrule matrix and chondrule rims. We submit that no artificial variations in IOM structure are introduced this way, since the elemental and N isotope compositions of these matrix-related petrological settings are undistinguishable (see Sections 3.1 and 3.2). Indeed, it has been suggested that textural differences between chondrule rims and intra-chondrule matrix are a consequence of aqueous alteration on the chondrite parent body (Brearley, 1993). For Bells, we targeted intra-chondrule matrix, whereas for Jbilet Winselwan, we selected domains from a chondrule rim as well as intra-chondrule matrix. These areas likely represent clasts of different lithologies. Maribo 'matrix' mostly consists of dust rims surrounding chondrules, Ca-Al-rich inclusions (CAIs), tochilinite and cronstedtite structures. The extracted ^{15}N-rich section from Maribo is derived from an intra-chondrule matrix-rich area not related but compositionally indistinguishable from the rim materials. The samples were then analyzed by a FEI Titan 80-300ST TEM, where bright field (BF) images were taken in STEM mode and STEM-EDS point analyses with a short dwell time (<5 s) were performed for the purpose of locating organic matter in the sections. These short dwell times cause negligible damage to the samples (van Kooten et al., 2017). Subsequently, EELS were collected in TEM diffraction mode, operating at 120 kV and using a beam diameter of 100 nm with a total acquisition time of 10–30 s. Using the TEM mode reduced significantly self-contamination of the sample during electron irradiation. We note that we observe no significant alterations to the organic fine-structure after STEM-EDS and TEM-EELS acquisitions, even after more extreme analytical conditions (van Kooten et al., 2017). A monochromator was used to obtain a high energy resolution of 0.1–0.2 eV, which provided distinct peak separations in carbon-K and nitrogen-K edges. The C-K and N-K edges were collected simultaneously over a range of 230–435 eV, with an energy step size of 0.1 eV. The backgrounds of these spectra were substracted using a power law and were normalized to the total carbon at 320 eV. To calculate the C/N ratios, we used the following equation from Lajaunie et al. (2015):

$$\frac{N_C}{N_N} = \frac{I_C}{I_N} \times \frac{\sigma_N}{\sigma_C}, \quad (1)$$

where the σ is the partial ionization cross section (calculated with Sigmak software in Fortran, with an energy window of 35 eV, a 120 keV incident beam and a 12.8 mrad collection angle) and I_C is the integral of the total carbon with an energy window of 285–320 eV and I_N is the integral of the total nitrogen with an energy window of 400–435 eV.

2.5. NanoSIMS

The TEM sections were analyzed by the ASIAA nanoSIMS (Academia Sinica, Taiwan) for investigation of the ^{15}N carrier. The samples attached to their copper TEM grids were gold coated (20 nm thickness) and subsequently deposited on double-sided sticky carbon pads. This procedure was necessary to achieve good charge compensation/dissipation in order to achieve the necessary count rates and MRP (>8000). Samples were pre-sputtered with a ~25 pA primary Cs^+ beam for ~15 min until sputter equilibrium was achieved. For analyses, a beam current of 1.0 pA was used, providing a spatial resolution of ~150 nm. The primary beam was rastered over 10 × 10 μm (256 × 256 pixels) with a dwell time of 2.5 ms/pixel, and we accumulated 20 repeated measurements (referred to as planes or cycles) on each area. The secondary ions of $^{16}O^-$, $^{12}C_2^-$, $^{12}C^{14}N^-$, $^{12}C^{15}N^-$ and $^{28}Si^-$ were measured in multi-collection mode. The results were processed using L'image software, including correction for detector deadtime (44 ns) and sample drift.

3. RESULTS

3.1. Mineralogy and composition of the CM chondrites

3.1.1. Maribo

EMPA. The Maribo section studied here has a homogeneous texture (i.e., we observe evenly distributed chondritic components and no signs of brecciation) and contains mainly chondrules (~10 vol%, chondrule rims not included), tochilinite and cronstedtite grains (~30 vol%) and rare CAIs surrounded by fine-grained dust rims (Fig. 1). The mineralogy of these dust rims is detailed in the section below. Chondrules are mainly porphyritic olivine types with minor Fe sulfides and sizes generally <500 μm in diameter. The chondrule mesostases consist of very fine-grained phyllosilicates. Large mm-sized metal grains such as observed in Paris are not present in either chondrule or matrix. This may indicate a higher degree of alteration relative to Paris, or alternatively, heterogeneous accretion of metal in CM chondrites. Indeed, it has been suggested that the high abundance of metal in Paris cannot be explained entirely by a low level of alteration (Hewins et al., 2014). Several cronstedtite and tochilinite textures are recognized, including fishbone tochilinite, compact tochilinite and cronstedtite, and irregular shaped cronstedtite (Haack et al., 2012). We analyzed the FeO/SiO_2 (3.8 ± 2.2, 1SD) and S/SiO_2 (0.7 ± 0.8, 1SD) ratios of compact cronstedtite ($n = 5$) and compact/fishbone tochilinite ($n = 5$) (Table 2), assuming PCP-like aggregates of 50% tochilinite and 50% cronstedtite (Haack et al., 2012). These values are similar to literature data of Maribo (Haack et al., 2012), confirming its low level of alteration (Fig. 2). Considering these ratios on the Rubin et al. (2007) scale of aqueous

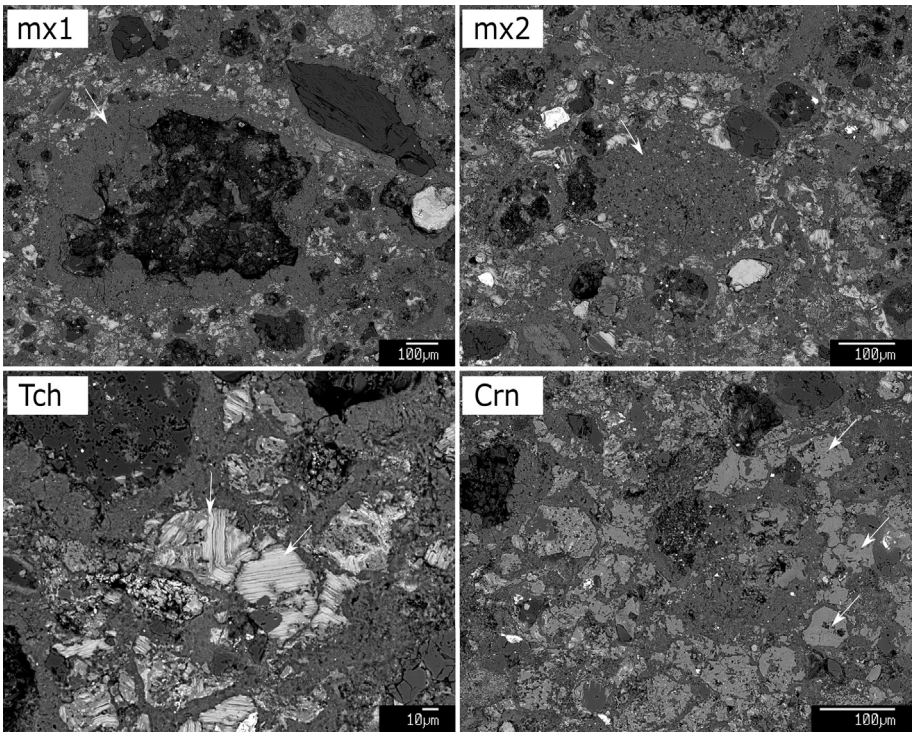

Fig. 1. BSE images of different matrix-rich regions of Maribo, on which EMP and SIMS analyses were done. Mx1 corresponds to a chondrule rim, whereas mx2 includes measurements on the matrix lump that is centred in the mx2 panel. Tochilinite (Tch) and cronstedtite (Crn) EMP analyses are from the grains shown in the lower two panels, which include fishbone Tch (arrows).

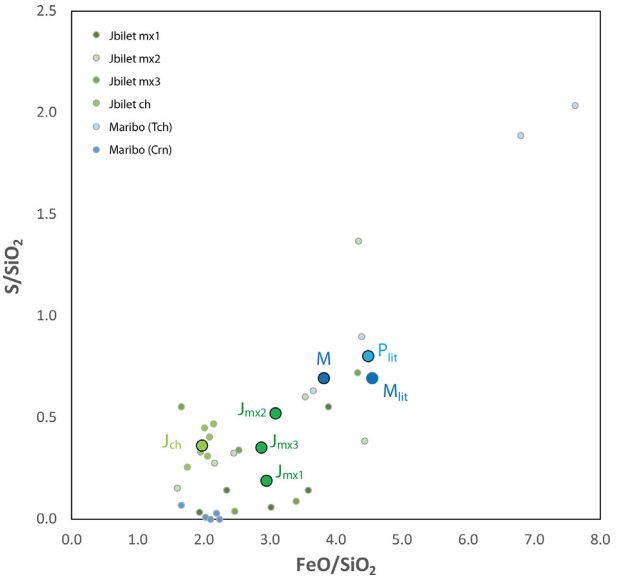

Fig. 2. FeO/SiO_2 versus S/SiO_2 ratios of tochilinite-cronstedtite intergrowths from Jbilet Winselwan as well as separate tochilinite and cronstedtite grains from Maribo. Small circles represent individual analyses, whereas large circles are averages of these analyses for different regions from Jbilet Winselwan (J, green) and Maribo (M, blue). Data is presented in Table 2. Also included are literature averages for Maribo (M_{lit}, Haack et al., 2012) and Paris (P_{lit}, Hewins et al., 2014).

alteration, the petrological type of Maribo is ~2.8. Naturally, assuming a lower tochilinite/cronstedtite ratio would result in a lower petrological grade. However, even with a very conservative percentage of 20 vol% tochilinite, the estimated petrological type is approximately 2.6. Hence, Maribo would still be considered among the least altered CM chondrites. Furthermore, detailed investigations of TCIs from Maribo show that their nanocrystalline texture and composition are in agreement with this assignation (Vollmer et al., 2014).

TEM. A ^{15}N-rich domain was extracted for TEM investigation from matrix region 2 (mx2). Compositions of minerals analyzed by STEM-EDS are presented in the Electronic Annex (Table 2 and Fig. 1). This domain is characterized by areas containing amorphous silicates and more abundant areas with a crystalline fine-grained matrix composed of TCIs interwoven with carbonaceous matter (Fig. 3A). The TCIs are typically tens of nanometers in length (Fig. 3C). Embedded in this matrix are some olivine crystals (~5 vol%), as well as iron sulfides (~5 vol%) and globular carbonaceous matter (<3 vol%). In addition, we find abundant small metal nugget clusters (<50 nm, ~5 vol%) relative to other CM chondrites, where the individual FeNi grains are coated by iron oxides (Fig. 3B). The preservation of these metal nuggets, which are unlike the large metal grains observed in the Paris matrix (Hewins et al., 2014), provides further evidence for the low degree of alteration in Maribo. We note that it is statistically not possible

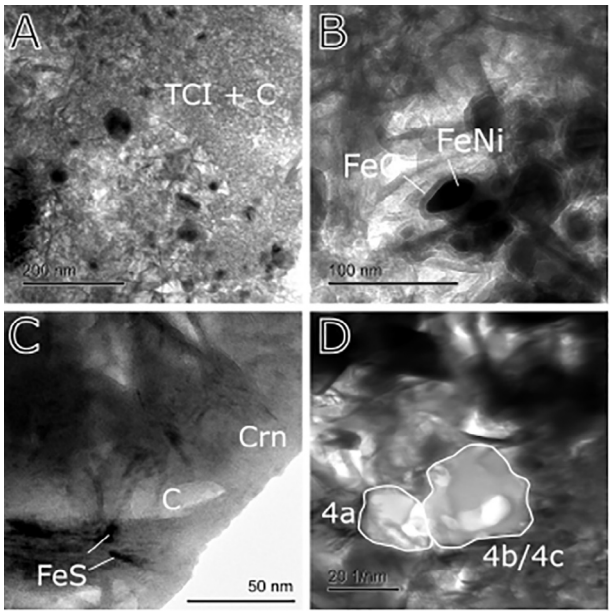

Fig. 3. BFSTEM images from a Maribo section extracted from mx2. (A) Overview image showing tochilinite-cronstedtite intergrowths (TCIs) interspersed by diffuse organic matter (C). (B) Small FeNi metal nuggets surrounded by iron oxide rims. (C) Zoom-in on interlayered Tch and Crn. (D) Globular organic matter from EELS4a and EELS4b.

to determine the overall abundance of metal in Maribo from a single TEM section and can, therefore, not compare to the Paris meteorite. Nevertheless, this TEM section indicates that Maribo may contain at least a similar amount of metal to Paris, albeit in smaller grain size.

3.1.2. Jbilet Winselwan

EMPA. Jbilet Winselwan consists of chondrules (~30 vol%), monomineralic chondrule fragments of magnesian olivine and pyroxene (~10 vol%), PCPs (~10 vol%), CAIs (~0.5 vol%) and matrix materials including dusty rims (~50 vol%). The chondrules (100–300 μm in diameter) have predominantly porphyritic olivine textures (PO, sometimes with pyroxene phenocrysts) and often contain abundant Fe oxides (Fig. 4). The porphyritic olivines are overprinted at the edges by coarse-grained phyllosilicates of which the mesostases consists. The chondrules are typically surrounded by one or more rims, where the innermost rim often consists of coarse-grained phyllosilicates and tochilinite and the outermost rim of finer-grained dust. The latter rim has higher total oxide weight abundances (~85 wt%) than the former rim (~80 wt%) (Table 1). In other chondrules, we observe single dust rims that increase in sulfide abundance and grain size further outwards, where the inner part of the rim is less altered. PCPs are typically surrounded by dust rims as well. Jbilet Winselwan is a breccia and some rounded clasts can be identified in the section that consist of more or less altered material than their surroundings. These

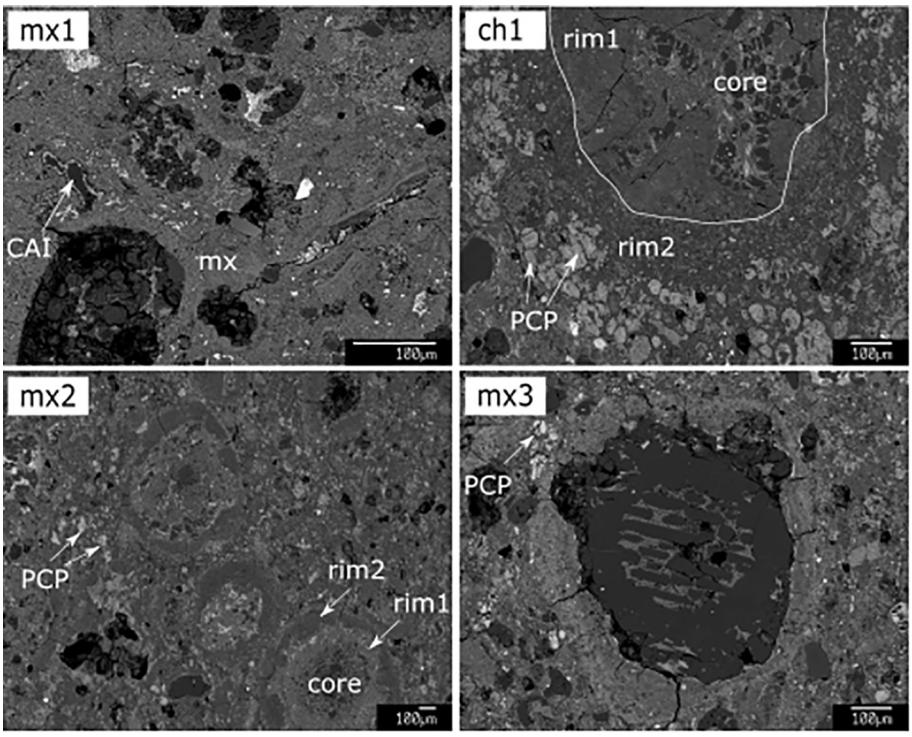

Fig. 4. BSE images of different matrix-rich regions of Jbilet Winselwan, on which EMP and SIMS analyses were done. Mx1 corresponds to intra-chondrule matrix, whereas mx2, mx3 and ch1 include measurements on chondrule rims and PCPs surrounding the chondrules. Data from these analyses are listed in Tables 1–4.

Table 1
Representative average compositions of matrices from Jbilet Winselwan, Bells and Maribo (in wt%). n = number of individual analyses, mx = matrix, ms = mesostasis.

		SiO_2	TiO_2	Al_2O_3	FeO	MnO	MgO	CaO	Na_2O	K_2O	Cr_2O_3	P_2O_5	S	NiO	Total	n
Jbilet Winselwan																
mx1	mx	26.8	0.1	2.1	34.8	0.3	14.0	0.9	0.8	0.1	0.4	0.3	2.1	2.0	84.5	6
mx2	1st rim	30.3	0.1	1.8	25.6	0.2	20.1	0.6	0.4	0.1	0.8	0.0	1.7	1.5	83.2	3
	2nd rim	32.0	0.1	2.4	22.2	0.2	17.6	0.7	0.4	0.1	0.6	0.1	1.6	2.2	80.2	5
	ms	29.1	0.0	1.4	26.7	0.1	22.5	0.5	0.3	0.1	0.6	0.0	2.2	1.4	84.9	1
mx3	rim	26.6	0.1	2.6	34.7	0.3	14.1	1.0	0.8	0.1	0.4	0.1	2.0	2.2	84.9	6
mx4	1st rim	30.5	0.1	2.1	24.0	0.2	17.1	1.0	0.6	0.1	0.6	0.1	3.0	2.2	81.6	8
	2nd rim	34.0	0.1	1.8	19.5	0.2	21.8	0.7	0.5	0.1	0.4	0.1	1.6	1.4	82.3	3
Bells																
mx1	mx	26.0	0.1	2.0	24.2	0.2	15.0	1.3	0.1	0.1	0.4	0.2	2.0	1.4	72.9	3
mx2	mx	23.9	0.1	2.0	26.0	0.2	13.4	1.7	0.2	0.1	0.3	0.2	2.2	1.3	71.5	4
ch1	rim	19.8	0.0	1.7	40.8	0.2	10.7	1.0	0.1	0.1	0.3	0.1	1.8	1.7	78.3	10
ch2	rim	23.8	0.1	2.1	30.8	0.3	10.6	1.6	0.1	0.1	0.3	0.2	2.6	2.1	74.8	5
Maribo																
mx1	rim	29.5	0.1	2.8	27.4	0.2	15.6	1.3	0.3	0.0	0.6	0.3	2.4	2.6	83.1	5
mx2	mx	28.4	0.1	2.9	27.9	0.3	14.9	1.9	0.3	0.0	0.5	0.7	2.9	2.9	83.7	5

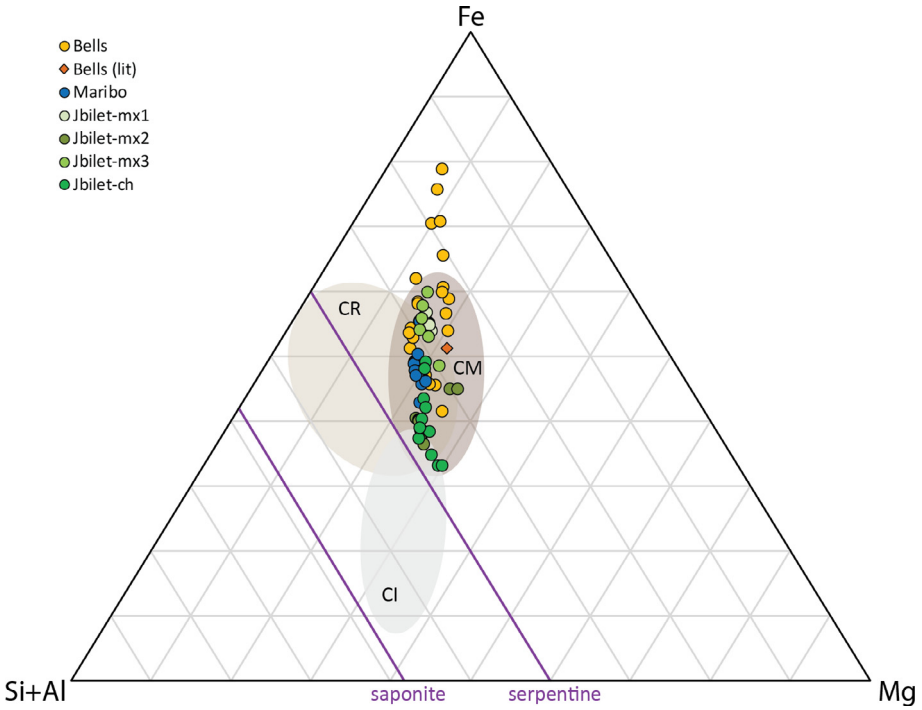

Fig. 5. Matrix compositions of Maribo, Jbilet Winselwan and Bells in ternary diagram with endmember compositions of relative abundances of Fe, Mg and Si + Al, calculated from their weight percentages. Data is presented in Table 1. Shaded ellipses represent compositional ranges from CR, CI and CM chondrites using data from Weisberg et al. (1993), Bunch and Chang (1980) and Tomeoka and Buseck (1988). Also given are solid solution lines for serpentine and saponite.

clasts show differences in matrix (Fig. 5, Table 1) and PCP (Fig. 2, Table 2) compositions. FeO/SiO_2 and S/SiO_2 ratios of PCPs in various regions of our Jbilet Winselwan section show that the degree of alteration ranges between petrological type 2.3 and 2.6 on the Rubin et al. scale. Averaged PCP compositions in three of the regions analyzed for N and H isotopes are nearly identical (FeO/SiO_2 = 2.9–3.1, S/SiO_2 = 0.3–0.5, Table 2) and are type 2.5–2.6. Note that these PCP compositions reflect average alteration indexes for an area in Jbilet Winselwan and that different degrees of alteration may still exist within that area (see Section 4.1). The matrix composition of these regions is more variable, specifically regarding their relative Fe-content (Fig. 5).

Table 2
Compositions of PCPs from Jbilet Winselwan, Bells and Maribo (in wt%).

	SiO_2	TiO_2	Al_2O_3	FeO	MnO	MgO	CaO	Na_2O	K_2O	Cr_2O_3	P_2O_5	S	NiO	Total
Jbilet Winselwan														
PCP (mx1)	15.1	0.0	2.9	54.1	0.3	7.0	0.3	0.4	0.1	0.1	0.0	2.1	2.4	84.9
PCP (mx1)	20.7	0.0	2.3	48.5	0.2	9.3	0.5	0.8	0.1	0.5	0.0	2.9	1.8	87.7
PCP (mx1)	16.6	0.1	1.9	49.9	0.2	9.2	0.4	0.3	0.0	0.1	0.1	1.0	2.4	82.2
PCP (mx1)	14.9	0.1	2.8	58.0	0.2	7.6	0.2	0.6	0.0	0.1	0.0	8.2	3.1	95.8
PCP (mx1)	25.4	0.1	4.0	49.0	0.3	9.6	0.3	0.9	0.1	0.2	0.0	0.9	0.7	91.5
PCP (mx2)	21.2	0.1	2.2	45.9	0.2	12.0	0.8	0.7	0.0	0.2	0.4	5.9	2.7	92.2
PCP (mx2)	13.1	0.0	1.8	58.0	0.2	7.8	0.3	0.3	0.1	0.1	0.0	5.0	2.3	89.1
PCP (mx2)	15.5	0.1	2.2	54.5	0.1	9.8	0.2	0.5	0.0	0.1	0.0	9.3	3.1	95.3
PCP (mx2)	10.3	0.0	1.0	44.8	0.2	7.7	0.5	0.3	0.1	1.5	2.0	14.2	13.4	96.1
PCP (mx2)	25.3	0.1	2.3	40.4	0.2	14.8	0.4	0.8	0.1	0.2	0.0	3.8	1.8	90.2
PCP (mx2)	19.6	0.1	2.2	48.2	0.2	11.3	0.3	0.6	0.0	0.1	0.0	6.4	2.1	91.1
PCP (mx3)	16.1	0.0	3.0	54.5	0.2	6.9	0.6	0.4	0.1	0.1	0.0	1.4	1.5	84.8
PCP (mx3)	21.7	0.0	1.5	36.1	0.2	14.3	0.2	0.5	0.1	0.2	0.0	12.0	5.5	92.3
PCP (mx3)	19.1	0.0	3.5	47.1	0.2	9.6	0.5	0.4	0.1	0.2	0.0	0.8	2.9	84.3
PCP (mx3)	13.3	0.0	2.3	57.5	0.1	7.3	0.5	0.5	0.1	0.1	0.0	9.6	2.8	94.2
PCP (mx3)	17.8	0.0	2.7	44.9	0.1	10.7	0.6	0.6	0.1	0.2	0.0	6.0	2.9	86.6
PCP (mx4)	22.1	0.0	2.3	45.9	0.2	12.4	0.2	0.7	0.1	0.0	0.0	8.9	1.7	94.6
PCP (mx4)	20.9	0.1	2.0	44.8	0.2	13.2	0.2	0.6	0.1	0.1	0.0	9.8	2.1	94.1
PCP (mx4)	21.4	0.0	2.0	43.0	0.2	12.6	0.2	0.5	0.0	0.1	0.0	9.6	3.0	92.6
PCP (mx4)	22.8	0.1	2.5	44.3	0.3	11.9	0.2	0.8	0.1	0.1	0.0	7.5	1.7	92.2
PCP (mx4)	24.2	0.1	2.5	42.4	0.2	12.9	0.2	0.8	0.1	0.1	0.0	6.2	1.8	91.5
PCP (mx4)	22.5	0.1	3.1	46.3	0.2	11.0	0.2	0.9	0.1	0.1	0.0	7.0	1.9	93.4
Maribo														
Crn	26.0	0.1	3.8	43.3	0.1	11.3	0.3	0.5	0.0	0.2	0.0	1.8	0.9	88.2
Crn	24.4	0.1	3.2	49.3	0.2	8.5	0.1	0.3	0.0	0.0	0.0	0.2	0.1	86.5
Crn	23.3	0.1	2.8	51.9	0.2	7.6	0.1	0.1	0.0	0.0	0.0	0.0	0.1	86.2
Crn	24.0	0.1	3.0	50.5	0.2	8.3	0.1	0.2	0.0	0.0	0.0	0.0	0.1	86.4
Crn	22.9	0.1	2.7	50.2	0.2	9.0	0.1	0.2	0.0	0.0	0.0	0.7	0.2	86.2
Tch	14.7	0.0	1.8	53.6	0.2	9.3	0.2	0.3	0.0	0.2	0.0	9.3	2.2	91.8
Tch	8.0	0.0	1.4	61.2	0.1	8.7	0.2	0.1	0.0	0.1	0.0	16.3	3.3	99.5
Tch	8.6	0.0	1.4	58.2	0.2	10.3	0.1	0.2	0.0	0.2	0.0	16.1	3.3	98.5
Tch	12.6	0.1	1.6	55.4	0.2	9.5	0.2	0.1	0.0	0.1	0.0	11.3	2.3	93.6

TEM. Two ^{15}N-rich domains (see Section 3.2) from Jbilet Winselwan were extracted for detailed investigation by TEM (see also Electronic Annex: Table 2 and Fig. 2 for mineral compositions). Both domains have PCP compositions corresponding to a petrological type of 2.5 (Fig. 2). The first domain is part of an outer chondrule rim from matrix region 2 (mx2), with a texture and mineralogy typical for the chondrules observed in this area of the Jbilet Winselwan thin section. BFSTEM images show that the texture of the FIB-extracted thin section is fairly homogeneous and consists of iron sulfides clustered with globular carbonaceous material embedded in a phyllosilicate matrix (Fig. 6A-C). The individual layers of these phyllosilicates are spaced 7 Å apart, corresponding to a serpentine structure typical for CM chondrites. Serpentine laths vary in size from tens to hundreds of nanometers and are interwoven with nonglobular carbonaceous matter. The second domain is extracted from matrix region 1 (mx1), where the intrachondrule matrix is rich in anhydrous silicates (mainly olivine) of <500 nm in diameter, cemented by matrix-like material (Fig. 6D-F). This matrix is composed of phyllosilicates interwoven with nonglobular carbonaceous material, where the spacing of the phyllosilicate layers (15 Å) corresponds to a saponite structure. Apart from the phyllosilicate structure, the matrix in mx1 is very similar to mx2, having globular carbonaceous matter and iron sulfides embedded as main minerals.

3.1.3. Bells

EMPA. The section of Bells investigated here is a porous aggregate of chondrules (~10 vol%), chondrule fragments (~10 vol%) and matrix materials (~70 vol%). The porosity of the Bells section is estimated to be 10–20% (using BSE images of the 1 × 1 cm section in ImageJ software), in agreement with previous porosity measurements (13%, Corrigan et al., 1997). Bells is more porous than Maribo and Jbilet, where we estimate the porosity to be <5%. We further observe dark clasts in Bells, which consist of a fine-grained matrix that is rich in sulfides. Other clasts in Bells contain chondrules surrounded by dust rims that are occasionally highly altered. TCIs and CAIs are absent, but atypically for CM chondrites we find a relatively high abundance of mm-sized FeNi metal and secondary phases such as Fe oxides and sulfides related to the metal

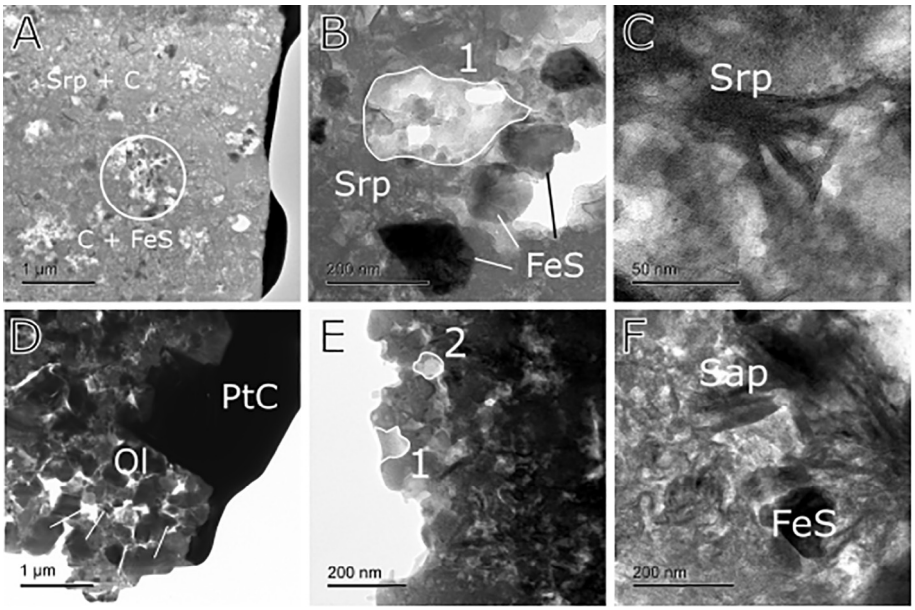

Fig. 6. BFSTEM images from Jbilet Winselwan sections extracted from mx2 (A-C) and mx1 (D-F). Mx2 has a homogeneous distribution of serpentine (Srp) interspersed with diffuse organic matter (C). Embedded in this matrix are clusters of iron sulfides (FeS) and carbonaceous globules. The globule in *B* is from EELS1. Mx1 is more crystalline than mx2 and contains abundant olivine crystals (Ol) embedded in a fine-grained matrix of saponite (Sap) and diffuse organic matter. Embedded in this matrix are organic globules (here imaged from EELS1 and EELS2) and sulfides. PtC = platinum carbon alloy.

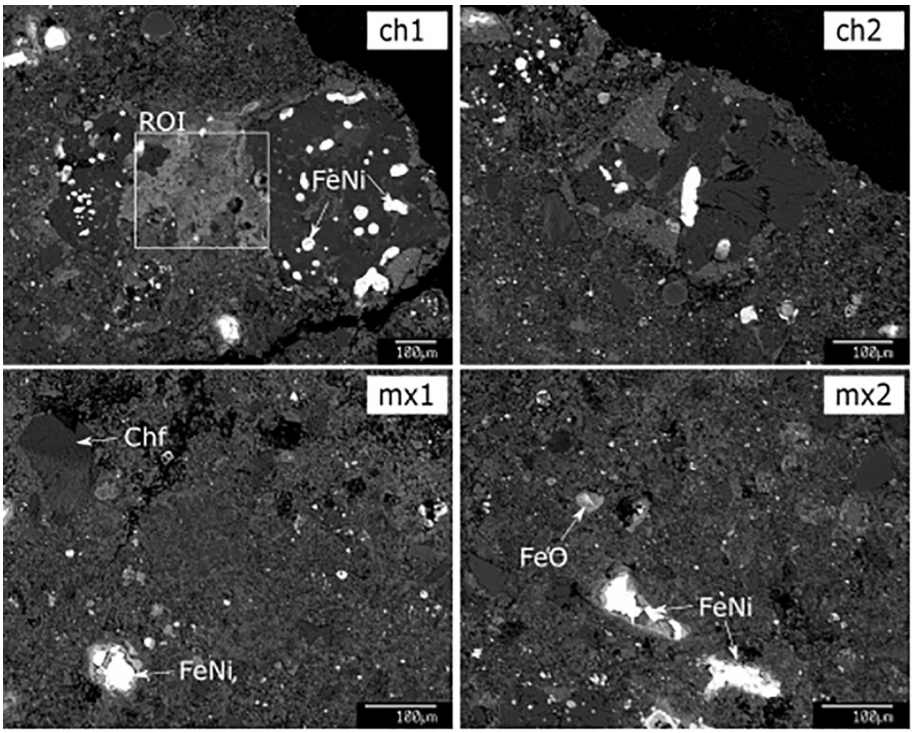

Fig. 7. BSE images of different matrix-rich regions of Bells, on which EMP and SIMS analyses were done. The region of interest (ROI) in area 'ch1' corresponds Fe-rich matrix between two chondrules. Ch2 includes analyses from the chondrule rim and surrounding matrix, mx1 and mx2 correspond to intra-chondrule matrix regions. FeNi metal is abundantly present within the chondrules and embedded in the matrix. This metal is often surrounded by iron oxides (FeO) or sulfides. Chf = chondrule fragment.

(~5 vol%, Fig. 7). Some of these oxides are present as fine-grained framboidal magnetite embedded between the phyllosilicates, whereas larger Fe oxides surround metal cores that are typically ~100 µm in diameter. Small cryptocrystalline and barred chondrules (<100 µm) are abundant (approximately 80 vol% of the total chondrules) and larger

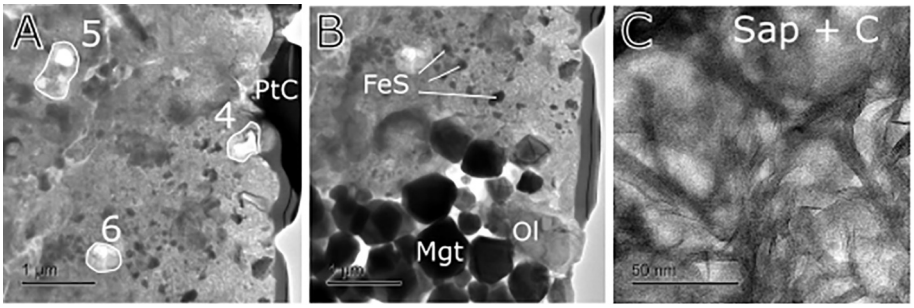

Fig. 8. BFSTEM images from a Bells section extracted from ch2. (A) Overview image showing multiple organic globules identified for EELS analyses. (B) Aggregate of magnetite (Mgt) embedded in a fine-grained matrix of (C) saponite (Sap) and diffuse organic matter (C).

chondrules (~500 μm) are typically porphyritic olivine and occasionally have dust rims. Both chondrule types as well as the chondrule fragments (generally consisting of single crystals or being cryptocrystalline) are highly magnesian with Mg#s > 90. The porphyritic chondrules typically contain abundant FeNi metal. Major element compositions matrix domains from Bells mostly overlap with those of other CM chondrites, but also consist of more Fe-rich compositions (Fig. 5, Table 1). Considering the petrological and chemical features of Bells that classify it as an anomalous CM chondrite, assigning a petrological type is challenging. Following the Rubin et al. (2007) scale, as done for Maribo and Jbilet Winselwan, we can also define the degree of alteration by the complexity of carbonates. Large PCPs are absent and carbonates are mainly complex with significant amounts of Fe and Mg. In summary, this suggests that at least the Bells matrix has a petrological type between 2.0 and 2.1. This high degree of alteration is in agreement with low totals observed for the Bells matrix (Table 1).

TEM. We extracted a ^{15}N-rich domain from the Bells matrix, which in BFSTEM mode is characterized by a region dominated by micron sized magnetite grains and a region occupied by fine-grained saponite (<100 nm) interwoven with carbonaceous matter (Fig. 8, see also Electronic Annex: Table 2 and Fig. 3 for mineral compositions). Globular carbonaceous and iron sulfide grains are abundantly embedded in this matrix and are typically <500 nm in diameter. While large metal grains (~100 μm) are abundant in the Bells matrix, there are no small scale grains found in the TEM section. The overal texture and mineralogy of this TEM section is in agreement with previous findings from Bells matrix (Brearley, 1995), which appears to be fairly homogeneous despite its brecciated nature and variations in Fe/Mg ratios.

3.2. N and C isotope compositions

SIMS. N and C isotope measurements were carried out on intra-chondrule matrix regions and chondrule rims of Maribo, Jbilet Winselwan and Bells (Table 3). Bulk C isotope images show a relatively narrow range of $\delta^{13}C$ values, with possibly more positive values for Maribo (average $\delta^{13}C = -15 \pm 13‰$), than for Jbilet Winselwan ($\delta^{13}C = -31 \pm 35‰$) and Bells ($\delta^{13}C = -21 \pm 10‰$). $^{13}C/^{12}C$ ratios are distributed fairly homogneously throughout the isotope image rasters and ^{13}C-rich domains are typically <500‰ for all CM chondrites studied here. The $\delta^{13}C$ value for Bells is in agreement with previous bulk analyses of this meteorite ($\delta^{13}C = -19.9‰$, Alexander et al., 2013). For Maribo, the averaged $\delta^{15}N$ value of all isotope images (n = 6) is 102 ± 66‰, similar to the average of Bells, where $\delta^{15}N = 97 \pm 51‰$ (n = 7, Table 3). This latter value is in agreement with previous SIMS analyses of Bells ($\delta^{15}N = 80–170‰$,

Table 3
Bulk nitrogen and carbon isotope data of intra-chondrule matrix (mx) and chondrule rim (rim) regions of Bells, Jbilet Winselwan and Maribo. Errors are presented in 2SE and are propagated errors from sample and Orgueil reference standard.

		$\delta^{13}C$ (‰)	$\delta^{15}N$ (‰)
Bells			
mx1#1	mx	−26 ± 18	109 ± 25
mx1#2	mx	−24 ± 14	109 ± 20
mx2#1	mx	−22 ± 11	115 ± 19
mx2#2	mx	−22 ± 16	124 ± 25
ch2#1	mx	−19 ± 18	55 ± 13
ch2#2	mx	−19 ± 16	70 ± 27
ch2#3	rim	−11 ± 22	98 ± 32
	average	−21 ± 10	97 ± 51
Jbilet Winselwan			
mx1#1	mx	−27 ± 35	44 ± 70
mx1#2	mx	−28 ± 27	47 ± 40
mx2#1	rim1	−30 ± 45	27 ± 61
mx2#2	rim1/2	−33 ± 30	38 ± 68
mx2#3	rim2	−32 ± 40	46 ± 96
mx2#4	rim2	−29 ± 42	54 ± 58
mx2#5	rim2	−32 ± 27	35 ± 90
mx3#1	rim	−31 ± 24	68 ± 89
mx3#2	rim	−34 ± 40	33 ± 84
	average	−31 ± 35	44 ± 73
Maribo			
mx1#1	rim	−7 ± 47	149 ± 79
mx1#2	rim	−13 ± 47	107 ± 67
mx2#1	mx	−14 ± 47	125 ± 33
mx2#2	mx	−14 ± 34	58 ± 91
mx3#1	mx	−12 ± 44	97 ± 63
mx3#2	mx	−27 ± 35	74 ± 46
	average	−15 ± 13	102 ± 66

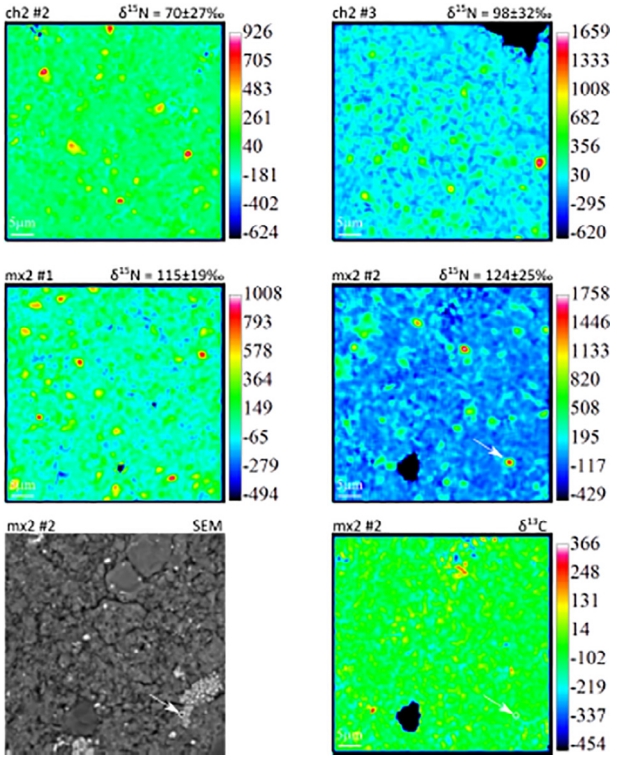

Fig. 9. $\delta^{15}N$ image rasters from 50 × 50 μm areas of Bells matrix. Bulk $\delta^{15}N$ values of the rasters are given above the images. The white arrow in mx2#2 represents the location of FIB-SEM extraction. The lower left panel shows the corresponding BSE image of raster mx2#2 and the lower right panel shows the corresponding $\delta^{13}C$ image.

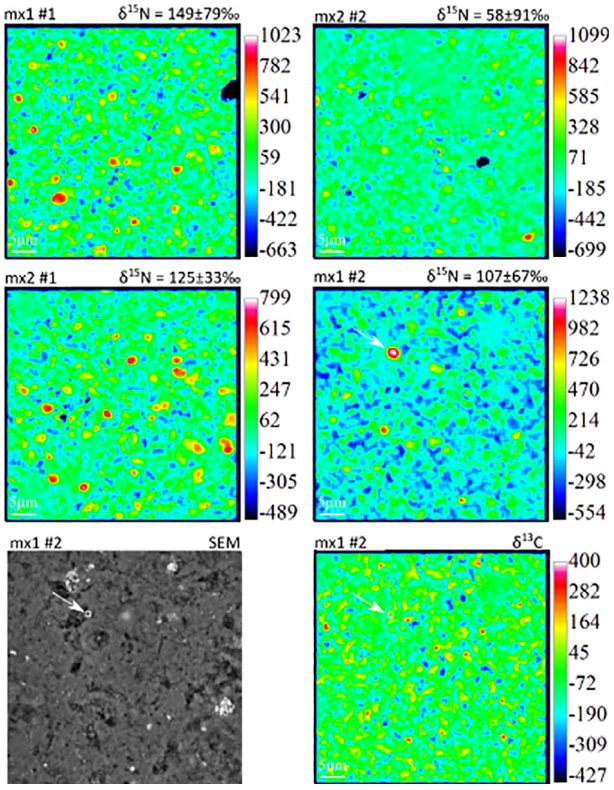

Fig. 10. $\delta^{15}N$ image rasters from 50 × 50 μm areas of Maribo matrix. Bulk $\delta^{15}N$ values of the rasters are given above the images. The white arrow in mx1#2 represents the location of FIB-SEM extraction. The lower left panel shows the corresponding BSE image of raster mx1#2 and the lower right panel shows the corresponding $\delta^{13}C$ image.

Messenger et al., 2008), but not with bulk ($\delta^{15}N = 353‰$) or IOM analyses ($\delta^{15}N = 415‰$) using gas spectrometry (Alexander et al., 2007, 2013). ^{15}N-rich domains in the Bells matrix are more enriched than in Maribo. For Bells we find hotspots up to ~2000‰ (Fig. 9), whereas ^{15}N-rich domains in Maribo are typically <1000‰ (Fig. 10). Both CM chondrites show no significant variations in N isotopes between intra-chondrule matrix and chondrule dust rims. Nitrogen isotope variations between different locations in the Maribo section are related to the amount of ^{15}N-rich domains in each raster image, which seem to be heterogeneously distributed (Fig. 10). A higher abundance of hotspots with $\delta^{15}N \approx 1000‰$ correlates with a higher bulk $\delta^{15}N$ value. For Bells, the $\delta^{15}N$ values for the hotspots are more variable, and areas with a higher abundance of hotspots correlate with lower $\delta^{15}N$ values for those hotspots (Fig. 9). Here, however, there seems to be no correlation between the amount of hotspots and the bulk $\delta^{15}N$ values of the raster images. This behaviour is also observed in N isotope images of Jbilet Winselwan (Fig. 11). Jbilet Winselwan has a lower average $\delta^{15}N$ value of $44 \pm 73‰$, equal to previously reported bulk values (Grady et al., 2014). The hotspot abundance correlates with a decrease in $\delta^{15}N$ values of these hotspots. We note that the ^{15}N-rich domains do not correlate with enrichments in ^{13}C (Figs. 9–11).

NanoSIMS. After detailed TEM investigations of the FIB-extracted CM chondrite regions, the Bells and Maribo sections were analyzed by nanoSIMS for the distribution of their N isotope composition – unfortunately the Jbilet Winselwan sections did not survive sample preparation (Fig. 12). We note that the $^{12}C^{14}N$ signal of certain low-carbon areas in the sections was below our designated counting threshold of 200 cts and, hence, only $\delta^{15}N$ values are visible in areas above this threshold. However, there are some significant observations that can be made with the data at hand. First, we can identify several organic globules in the Bells section using $^{16}O^-$ and $^{12}C_2^-$ isotope images (white circles, Fig. 12). Some of these globules correlate with the most ^{15}N-rich areas in the section, with $\delta^{15}N$ values < 1600‰, similar to the hotspot anomaly determined by UH ims-1280 (Fig. 9). These observations are in agreement with previous nanoSIMS analyses of Bells (Messenger et al., 2008; De Gregorio et al., 2013), showing that the carrier of ^{15}N in Bells is typically located in globular IOM, although not all globules are ^{15}N-rich. Some globules from the Maribo TEM section are enriched relative to the bulk section ($\delta^{15}N$ ~100‰). However, similar enrichments ($\delta^{15}N$ ~600‰) are also observed in non-globular carbonaceous matter.

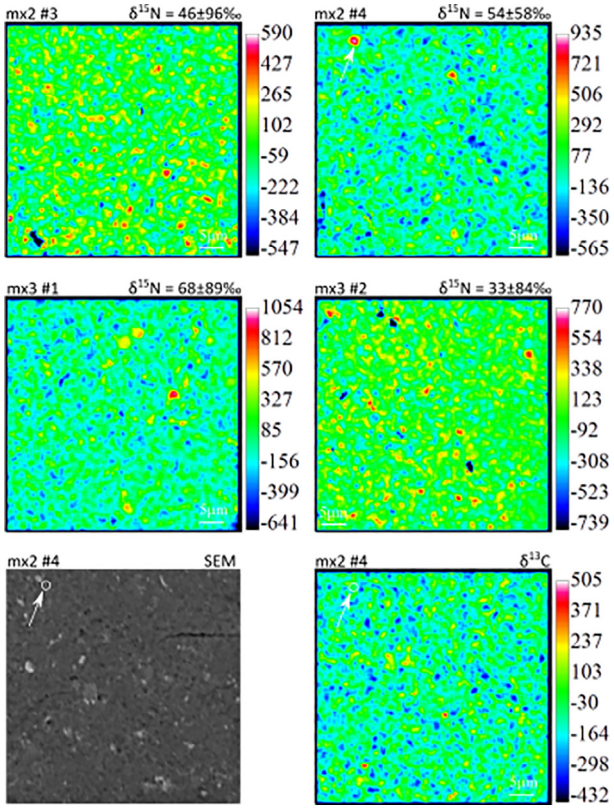

Fig. 11. $\delta^{15}N$ image rasters from 50×50 μm areas of Jbilet Winselwan matrix. Bulk $\delta^{15}N$ values of the rasters are given above the images. The white arrow in mx2#4 represents the location of FIB-SEM extraction. The lower left panel shows the corresponding BSE image of raster mx2#4 and the lower right panel shows the corresponding $\delta^{13}C$ image.

3.3. H isotope compositions

Measurements of H isotopes by UH ims-1280 using an O^- primary beam give information on the D/H ratio of phyllosilicates in chondrite matrices, with a negligible contribution from the organic matter (Deloule and Robert, 1995; Bonal et al., 2010; Piani et al., 2012). Measuring the D/H ratio of the phyllosilicates provides useful information about aqueous alteration, since it reflects an exchange between the relatively D-poor component of the water-rich altering fluid and the D-rich organic matter (van Kooten et al., 2017). The analyses of D/H by Cs^+ primary beam contributes additional hydrogen ionization from the organic matter, thus resulting in a total hydrogen isotope signature from phyllosilicates (e.g., a two-component mixture) and organic matter. The robustness of using this method as a means to establish a relationship to the level of aqueous alteration in chondrites is challenged by the unknown ratio of phyllosilicates/organics in the sample. Alexander et al. (2012) suggested that trends between D/H and C/H reflect mixing lines between D-poor water and D-rich IOM assuming all carbon is incorporated in this organic matter. Hence, the C/H ratio can be used as a proxy for the level of hydration. However, as additionally noted by these authors, carbon is also incorporated in carbonates and SOM, which may obscure the mixing of a two-component system. Although the ionization efficiency of carbonates has been deemed negligible (Wiliford et al., 2016), the ionization efficiency of the SOM when using a Cs^+ primary beam may be significant (see Section 4.1). Here, we focus on a simpler approach using an O^- primary beam as well as measuring C/H and Si/H ratios to determine the level of alteration in our samples (Section 4.3). Hydrogen isotope analyses of three CM chondrites were carried out in close proximity to areas where C-N isotope

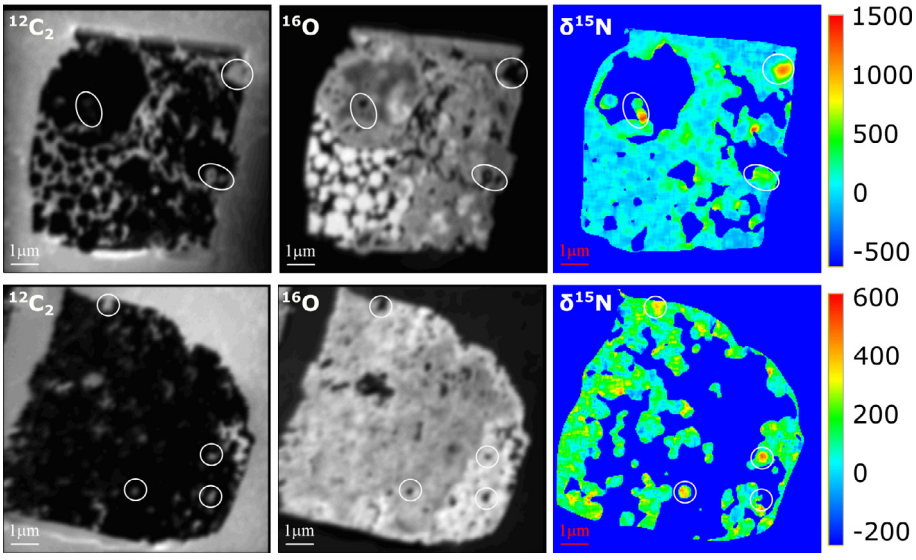

Fig. 12. $^{12}C_2$, ^{16}O and $\delta^{15}N$ nanoSIMS images of Bells (upper panels) and Maribo (lower panels) TEM sections. White circles indicate globular organic matter, with high C/O ratios.

Table 4
H isotope and $^{13}C/H$ compositions of matrix regions from Orgueil, Bells, Jbilet Winselwan and Maribo analyzed by SIMS.

		D/H	δD (‰)	$^{13}C/H$
Orgueil				
#1	mx	1.49E−04 ± 6.41E−06	−43 ± 41	2.14E−04
#2	mx	1.45E−04 ± 7.11E−06	−66 ± 46	2.32E−04
#3	mx	1.46E−04 ± 1.43E−05	−63 ± 92	2.42E−04
#4	mx	1.43E−04 ± 1.25E−05	−80 ± 80	2.01E−04
	average	1.46E−04 ± 4.85E−06	−63 ± 31	2.61E−04
Bells				
mx1#1	mx	1.27E−04 ± 6.87E−06	−185 ± 44	1.62E−04
mx1#2	mx	1.37E−04 ± 9.17E−06	−121 ± 59	2.16E−04
mx1#3	mx	1.25E−04 ± 4.58E−06	−199 ± 29	3.04E−04
mx2#1	mx	1.35E−04 ± 5.89E−06	−134 ± 38	2.30E−04
mx2#2	mx	1.41E−04 ± 7.39E−06	−93 ± 47	2.39E−04
mx2#3	mx	1.35E−04 ± 6.20E−06	−131 ± 40	2.24E−04
mx2#4	mx	1.32E−04 ± 6.43E−06	−156 ± 41	2.16E−04
	average	1.33E−04 ± 1.16E−05	−146 ± 75	2.27E−04
Jbilet Winselwan				
mx1#1	mx	1.08E−04 ± 4.02E−06	−307 ± 26	8.43E−05
mx1#2	mx	1.07E−04 ± 7.08E−06	−316 ± 45	7.13E−05
mx1#3	mx	1.08E−04 ± 6.64E−06	−304 ± 43	8.40E−05
mx1#4	mx	1.05E−04 ± 7.74E−06	−328 ± 50	7.55E−05
mx1#5	mx	1.09E−04 ± 6.70E−06	−301 ± 43	7.05E−05
	average		−311 ± 22	
mx2#1	rim2	1.20E−04 ± 6.08E−06	−230 ± 39	1.28E−04
mx2#2	rim2	1.21E−04 ± 8.26E−06	−220 ± 53	1.15E−04
mx2#3	rim2	1.19E−04 ± 5.52E−06	−238 ± 35	1.07E−04
mx2#4	rim1	1.10E−04 ± 6.03E−06	−296 ± 39	5.26E−05
mx2#5	rim2	1.18E−04 ± 5.87E−06	−245 ± 38	1.21E−04
mx2#6	rim2	1.17E−04 ± 6.26E−06	−250 ± 40	1.39E−04
	average	1.13E−04 ± 1.24E−05	−276 ± 78	9.53E−05
Maribo				
mx1#1	rim	1.09E−04 ± 6.37E−06	−302 ± 41	6.09E−05
mx1#2	rim	1.06E−04 ± 4.40E−06	−320 ± 28	5.66E−05
mx1#3	rim	1.03E−04 ± 5.35E−06	−341 ± 34	5.43E−05
mx1#4	rim	1.05E−04 ± 5.70E−06	−327 ± 37	6.26E−05
mx2#1	mx	1.11E−04 ± 5.80E−06	−288 ± 37	5.53E−05
mx2#2	mx	1.14E−04 ± 5.00E−06	−269 ± 32	6.49E−05
mx2#3	mx	1.10E−04 ± 9.69E−06	−294 ± 62	5.98E−05
mx2#4	mx	1.05E−04 ± 1.79E−05	−325 ± 115	5.77E−05
mx2#5	mx	1.11E−04 ± 9.29E−06	−289 ± 60	8.96E−05
mx2#6	mx	1.06E−04 ± 5.65E−06	−317 ± 36	8.34E−05
	average	1.08E−04 ± 6.95E−06	−307 ± 45	6.45E−05

images were obtained (Table 4). The δD values of Maribo, Jbilet Winselwan and Bells range between −341 ± 47‰ and −93 ± 47‰, in agreement with previous SIMS analyses of CM chondrite matrices (Piani et al., 2018). Maribo has the most negative δD values, averaging around −307 ± 45‰ (2SD) and Bells the least negative, with δD = −146 ± 75‰. Jbilet Winselwan D/H ratios vary for different clast regions, with matrix region 1 (mx1, Fig. 4) consisting of intra-chondrule matrix being more negative (δD = −311 ± 22‰) than matrix region 2 (mx2, Fig. 4), which consists of chondrule rim material (δD = −247 ± 53‰).

3.4. Structure of organic matter

EELS C-K edges and N-K edges were analyzed in carbonaceous grains in TEM sections from Maribo, Jbilet Winselwan and Bells (Fig. 13). The N-K edges reported here are from the same acquisition as the C-K edges. To avoid spectra with low signal/noise ratios, we selected N-K edges with π^* transition peaks > 0.003 (arbitrary normalized units).

3.4.1. Maribo

Maribo consists of carbonaceous grains that are more or less globular (i.e., with a rounded shape, but somewhat elongated or with irregular boundaries) and are composed of a singular smooth grain without core and rim morphology. The carbon structure in the π^* transition is very uniform for all four grains analyzed and shows a distinct peak at 285 eV, corresponding to aromatic and olefinic carbon (e.g., C=C). A smaller peak is located at 286.5 eV and is associated with aldehyde/ketone bonding structures

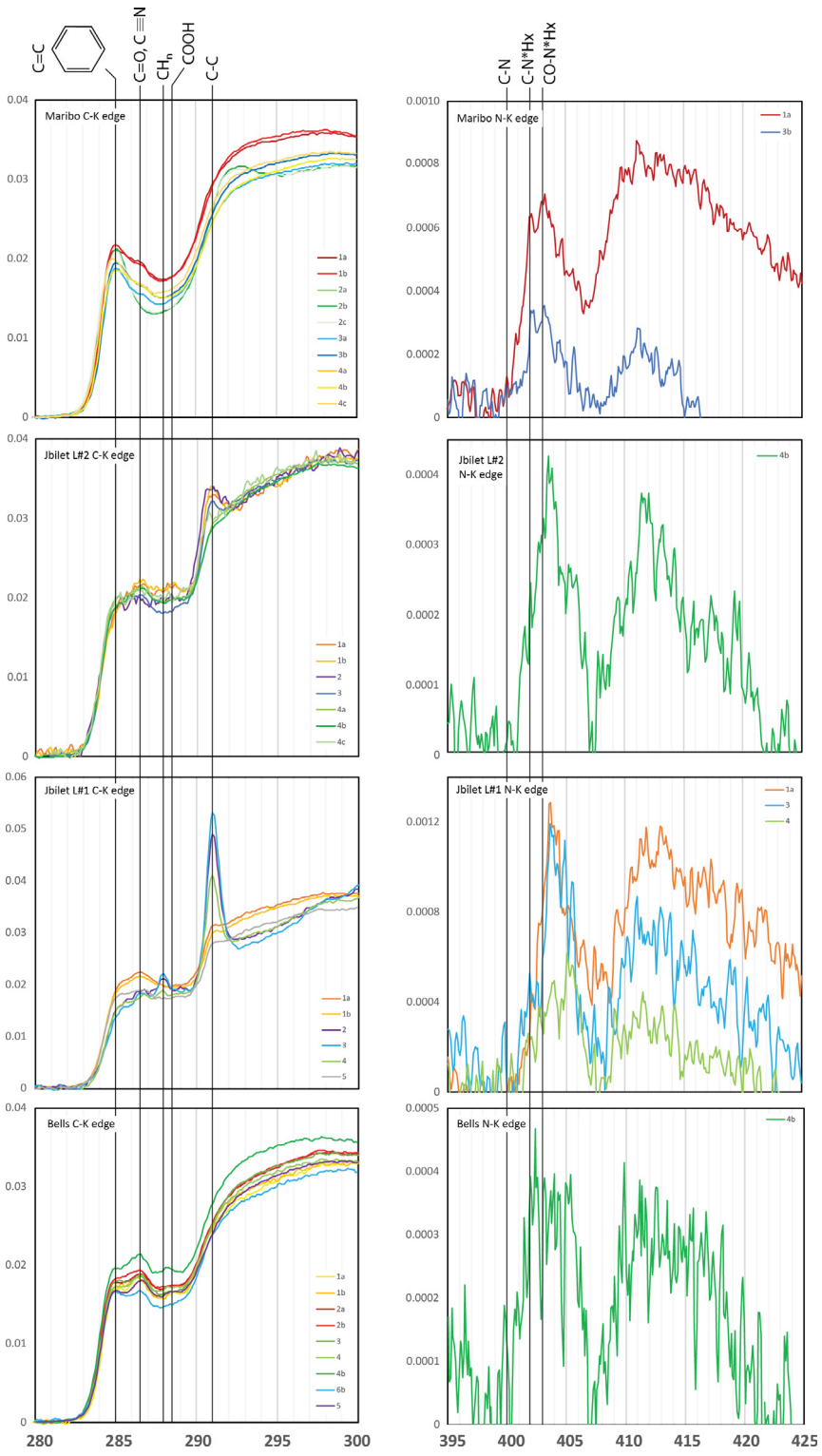

Fig. 13. EELS C-K (left column) and N-K edges (right column) of Maribo, Jbilet Winselwan (L#1 = mx1, L#2 = mx2) and Bells, all normalized to total carbon (320 eV) and nitrogen (430 eV). Peak positions are from Cody et al. (2008), where in the π^* transition (1) ~285 eV is associated with aromatic or olefinic carbon (C═C); (2) ~286.5 eV is associated with carbonyl/ester (C═O) and ether groups, (C─O) in aldehydes and ketones, as well as nitrile bonding (C≡N) environments; (3) ~287.5 eV corresponds to aliphatic carbon; (4) ~288.5 eV is associated with carbonyl groups in carboxyl moieties (COOH) and (5) ~291 eV corresponds to C─C bonding environments in graphene carbon ring structures. Peaks in the N-K edges correspond to: (1) ~400 eV nitrile functional groups (C≡N); (2) The broader peaks between ~403–407 eV belong to amine functional groups in imidazole and pyrrole and the broad peak starting at ~411 eV is related to amine functional groups in imidazole. Sharp peaks at 402 and 403 eV are associated with C─NH and CO─NH bonding environments.

(e.g., C═O). The N-K edge structure was obtained from two out of four grains and in both we distinguish peaks at 402 and 403 eV in the π^* transition, which correspond to C─NH and CO─NH bonding environments. From C-K and N-K edges, we calculated the C/N ratios of the grains, which are found to be >30.

3.4.2. Jbilet Winselwan

Individual carbonaceous grains from Jbilet Winselwan mx1 and mx2 are more often found as organic aggregates, but generally have similar sizes and globular morphologies as grains from Maribo. However, they are in many cases altered by phyllosilicate overgrowths. C-K edges from the mx2 region show a π^* transition of continuous intensity, with small peaks at 286.5 eV and 288.5 eV, the latter corresponding to carboxyl bonding environments (e.g., COOH). Another peak is found in the σ^* transition at 291 eV and is associated with graphene or polycyclic aromatic hydrocarbons. The C-K edges of the mx1 region have a similar structure, but for a notable increase in the 291 eV peak as well as a shift from the 288.5 eV peak to 288 eV, which reflects an increase of C─NH and a decrease in COOH functional groups. For both matrix regions, the N-K edges are very similar to the Maribo N structure, with a peak at 403.5 eV. These structures correlate well with organic compounds related to C─NH functional groups (Franke et al., 1995). Although statistically uncertain, C/N ratios of mx2 appear higher (C/N > 126) than mx1 (C/N > 25).

3.4.3. Bells

Carbonaceous grains from Bells are more globular compared to Maribo and Jbilet Winselwan (i.e., more rounded and with less irregular boundaries) and have core and rim structures, ranging in size between ~100 and 500 nm. The C-K edge structures of the grains are uniform with the highest peak intensity at 286.5 eV and 288.5 eV, similar to carbon bonding environments seen in Jbilet Winselwan mx2. The π^* transition of the N-K edge is more broadly distributed around 403.5 eV. C/N ratios are >118.

4. DISCUSSION

4.1. N isotope variability of CM chondrites: implications for heterogeneous accretion of ^{15}N-carriers

Nitrogen isotope images of Bells and Jbilet Winselwan show similar behaviour patterns in that a higher abundance of ^{15}N-rich domains correlates with lower δ^{15}N values for these hotspots. We suggest these N isotope patterns for Bells and Jbilet Winselwan are best explained by aqueous alteration processes, which decrease the magnitude of the ^{15}N-rich domains and homogenize the N isotope signatures throughout the matrix. Hence, the most unaltered regions in Jbilet Winselwan and Bells are characterized by hotspots with the highest δ^{15}N values, which are ~1000‰ and ~2000‰, respectively. Maribo, however, has relatively consistent ^{15}N enrichments in the hotspot domains, which are heterogeneously distributed over the matrix. This suggests that Maribo, in agreement with its mineralogy (see Section 3.1.1), has experienced less aqueous alteration than Jbilet Winselwan and Bells. We note that the ^{15}N-rich domains in Maribo correlate in magnitude with the most ^{15}N-rich hotspots of Jbilet Winselwan, suggesting that Jbilet Winselwan is simply a more altered CM chondrite than Maribo. Although within Bells we find N isotope patterns related to aqueous alteration, the overall higher ^{15}N enrichments of Bells relative to Maribo, a less altered CM chondrite, cannot be explained by redistribution of N through aqueous alteration.

Average bulk δ^{15}N values of CM chondrites range between −15‰ and +15‰ (Alexander et al., 2013). Nitrogen isotope signatures for IOM of the same meteorites have a similar range, between −10 and +10‰ (Alexander et al., 2007). Recently, the least altered CM chondrite Paris was found to have a bulk δ^{15}N value of +19.5‰ (Vinogradoff et al., 2017), on the upper end of CM chondrite values. Bells, often described as an anomalous CM chondrite (Kallemeyn, 1995; Mittlefehldt, 2002), has reported bulk and IOM δ^{15}N values of 353‰ and 415‰, respectively. However, SIMS analyses (this work and Messenger et al., 2008) consistently give lower bulk values of 80–170‰. In addition, the Maribo bulk average δ^{15}N value measured by SIMS is significantly higher than that of Paris although these CM chondrites are similarly altered and Paris perhaps even less (Hewins et al., 2014). Previous nanoSIMS analyses of bulk IOM from Bells and CR chondrite TEM sections have shown that the porous and ultramicrotomed IOM can absorb a large amount of terrestrial N_2 (40–70%) that is only removed by significant presputtering (De Gregorio et al., 2013) and can thus have consistently lower the δ^{15}N values with respect to the actual values. However, our SIMS measurements were done on thick sections that are presputtered at intensities that are an order of magnitude longer and more intense relative to that typically done by nanoSIMS. Moreover, these sections are not as porous as the IOM containing TEM sections and our SIMS analyses do not appear to give consistently lower δ^{15}N values than gas spectrometer analyses, as evidenced by Maribo, Jbilet Winselwan and Bells. If our samples were consistently contaminated with terrestrial N_2, this would suggest that Maribo has a similar δ^{15}N bulk value as Bells and that Jbilet Winselwan would be significantly enriched in ^{15}N compared to other CM chondrites as well. However, we know from bulk N isotope measurements of Jbilet Winselwan, that this CM chondrite has a lower δ^{15}N value than our SIMS analyses (Grady et al., 2014). Therefore, we provide an alternative explanation for our samples and suggest that this discrepancy is the result of variations in the ionization efficiency of organic components with different N isotope signatures. In chondrites, the two main organic components are SOM (~30 vol%) and IOM (~70 vol%, Pizzarello et al., 2006). Assuming all nitrogen is contained in these two components, the SOM of Bells should be depleted in ^{15}N relative to its IOM, since the measured IOM δ^{15}N value is higher than the bulk Bells value (Alexander et al., 2007, 2013). A simple mass balance calculation shows that the SOM δ^{15}N value of Bells should be ~150‰, in agreement with the SIMS analyses. SOM, including amino acids of typical CM chondrites such as Murchison, have measured

$\delta^{15}N$ values between 70‰ and 180‰ (Becker and Epstein, 1982; Elsila et al., 2012), within range of Maribo bulk SIMS analyses. Collectively, this suggests that perhaps the ionization efficiency of SOM is larger than that of IOM and, therefore, N isotope measurements by SIMS give a less representative picture of bulk values than previously thought.

If correct, this suggests that the SOM $\delta^{15}N$ composition of Bells, Jbilet Winselwan, Maribo and other CM chondrites (including Murchison) is very similar, in agreement with the identification of SOM organic moieties in Bells (Monroe and Pizzarello, 2011). The anomalous nature of Bells relative to CM chondrites with a more or less terrestrial bulk $\delta^{15}N$ composition is then best explained by changes in the N isotope composition of IOM-like organic matter. Based on these results, we suggest that relatively small variations in $\delta^{15}N$ between CM chondrites in the order of tens of permil are related to parent body alteration processes (e.g., Maribo and Jbilet Winselwan). Large variations in the order of hundreds of permil between different chondrite groups must be related to heterogeneous accretion of ^{15}N-carriers located in either IOM or SOM. For example, it is suggested that correlated increases of $\delta^{15}N$ and δD in IOM of carbonaceous chondrites are the result of increased isotope fractionation in organic ices with time in cold interstellar environments (Aléon, 2010). Hence, CR chondrites and Bells likely accreted more mature IOM than other carbonaceous chondrites. We speculate that Bells represents CR-like material that accreted late onto the CM chondrite parent body, thereby explaining characteristics similar to CM (i.e., O and H isotope composition, noble gas signatures and bulk elemental composition) and CR chondrites (i.e., IOM composition, metal abundance).

4.2. Hisotope behaviour during aqueous alteration

We show in Fig. 14 the D/H ratios of Maribo, Jbilet Winselwan and Bells against their $^{28}Si^+/H^+$ and $^{13}C^+/H^+$ ratios, of which the latter is determined using the bulk $^{13}C/^{12}C$ and $^{12}C/H$ ratios analyzed by SIMS. The CI chondrite Orgueil was measured under the same analyzing conditions as the CM chondrites and is also plotted. A regression through all data (except Jbilet Winselwan mx1) yields positive correlations between D/H versus $^{28}Si^+/H^+$ and $^{13}C^+/H^+$ ratios. We note that Jbilet Winselwan mx1 – as indicated by its mineralogy and texture (Section 3.1.2) – likely experienced secondary thermal metamorphism resulting in hydrogen loss as shown in Fig. 14a. We show that using $^{28}Si^+/H^+$ (Fig. 14a) instead of $^{13}C^+/H^+$ (Fig. 14b) as a proxy for the level of hydration yields a less scattered regression ($r^2 = 0.88$) as well as a more negative intercept for the D/H ratio. These intercepts are interpreted as the H isotope compositions of the altering fluid (van Kooten et al., 2017) and translate to a δD of -637 ± 64‰ and -384 ± 40‰ for using $^{28}Si^+/H^+$ and $^{13}C^+/H^+$, respectively. Even though different measuring techniques are used (see Section 3.3), this latter δD value correlates well with the value found by Piani et al. (2018) for a suite of typical CM chondrites ($\delta D = -350$‰) and also using the $^{13}C^+/H^+$ ratio as a proxy for the level of hydration.

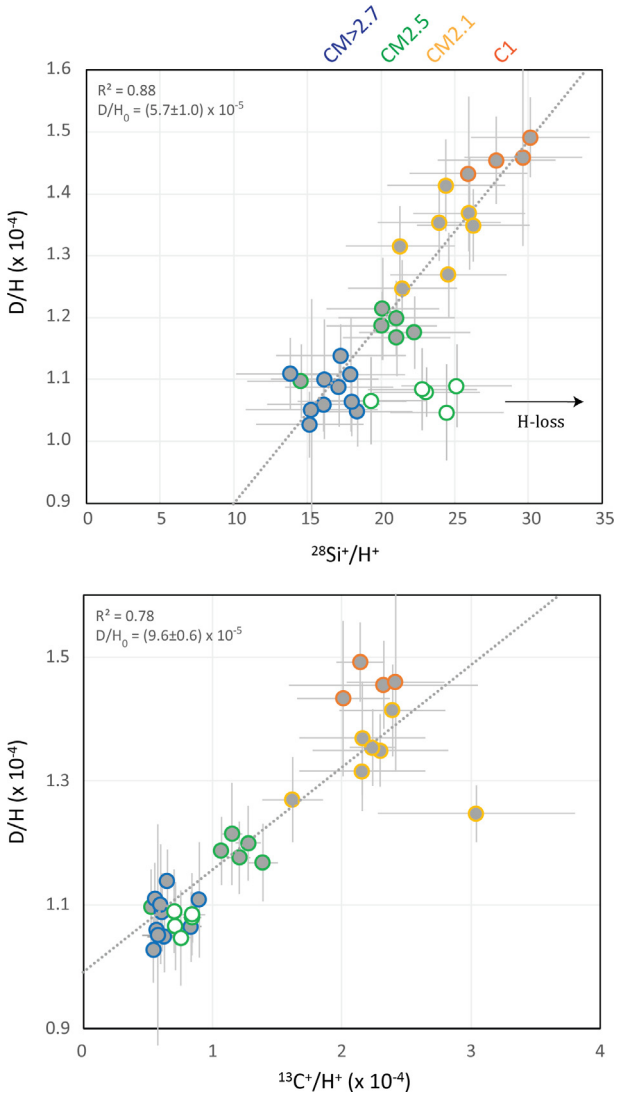

Fig. 14. (a) D/H versus $^{28}Si^+/H^+$ ratios and (b) D/H versus $^{13}C^+/H^+$ ratios of CM chondrites. Datapoints are for Maribo (blue), Jbilet Winselwan (green, mx1: open circles and mx2: closed circles), Bells (yellow) and Orgueil (orange). The regressions through these data are represented by the dashed lines and intercepts are provided in the plot (D/H_0).

However, a more negative δD value for the composition of the altering fluid on the CM chondrite parent body ($\delta D = -676$–493‰) was inferred from a detailed study of bulk Fe valence state in CM chondrites (Sutton et al., 2017).

The positive trends shown in Fig. 14 are suggested to reflect mixing between a D-poor water reservoir and a D-rich organic reservoir (van Kooten et al., 2017). If correct, the more altered CM chondrites should lie downslope of the trend, whereas more pristine samples should be more D-rich. Curiously, Maribo is more D-poor than the more altered CM and CI chondrites. The most straightforward explanation is that Bells and certain clasts of Jbilet Winselwan are less altered than Maribo. Although certain clasts in Jbilet Winselwan may indeed be quite unaltered (Russell

et al., 2014), this would be in complete contrast to mineralogical and compositional features observed in clasts from this work, as well as oxygen isotope and noble gas signatures of Maribo. Furthermore, we have plotted D/H ratios of the CI chondrite Orgueil in Fig. 14, showing that the highly altered CI chondrite has similar $^{13}C^{+}/H^{+}$ ratios as Bells. Hence, it is highly unlikely that Maribo is more altered than either Jbilet Winselwan or Bells. We discuss below three alternative mechanisms that can potentially explain the reversed correlation that we observe, including H-loss and consequent H isotope fractionation by (1) Fe oxidation, (2) serpentinization and (3) TCI decomposition.

4.2.1. H_2 release during Fe oxidation

Recently, the oxidation of Fe metal in chondrites during aqueous alteration was proposed to account for an increased D/H ratio of the residual water composition (Alexander et al., 2015; Sutton et al., 2017) according to the following reaction:

$$3Fe + 4H_2O \rightleftharpoons Fe_3O_4 + 4H_2(g) \quad (1)$$

The release and removal of D-poor H_2 gas during this process would result in increasingly D-rich residual water. This water would then react with anhydrous silicates to form phyllosilicates. Hence, depending on the initial metal and water content of a chondrite, an increased D/H ratio would be observed with increasing amount of Fe oxidation. There are several complications to this model: (1) Besides Fe oxidation reactions, the D/H ratio of water will also change during mixing with D-rich organic matter (Alexander et al., 2012). Dependent on the order of these processes one would expect different trend lines (Fig. 15). For example, if Fe oxidation occurs before the water mixes with hydrogen from organic matter, a negative correlation is expected between D/H and $^{13}C^{+}/H^{+}$ ratios. Indeed, during the onset of aqueous alteration, Fe metal is one of the first components to be altered to secondary oxide or sulfide phases. Hence, during Fe oxidation the D/H ratios do not neccesarily increase together with progressive alteration. (2) Fe oxidation processes may not be enough to account for the amount of H isotope fractionation observed between Maribo, Jbilet Winselwan and Bells. The amount of H isotope fractionation that will occur during Fe oxidation is dependent on the initial amount of Fe metal in the chondrite, the initial water/rock ratio, the amount of Fe metal that reacts to FeS instead of FeO and other oxidation processes that can convert water to H_2 gas. We assume that the initial amount of metal in CM chondrites is similar to the most unaltered regions of Paris (3 wt%), which would be conservative since the high abundance of metal in Paris is likely related to heterogeneous accretion of metal relative to other CM chondrites (Hewins et al., 2014). Taking another conservative estimation of the initial water/rock ratio of CM chondrites of ~20 wt% (Garenne et al., 2014) and assuming all metal reacts to form oxides, the maximum percentage of the total water reacted to H_2 gas would be ~12% (see appendix A). Using a lower amount of Fe metal or a higher water/rock ratio would only decrease this fraction. Consequently, if the initial D/H ratio is 1.00×10^{-4}, then the maximum fractionation can only amount to $D/H = 1.08 \times 10^{-4}$, significantly lower than D/H ratios of Bells matrix.

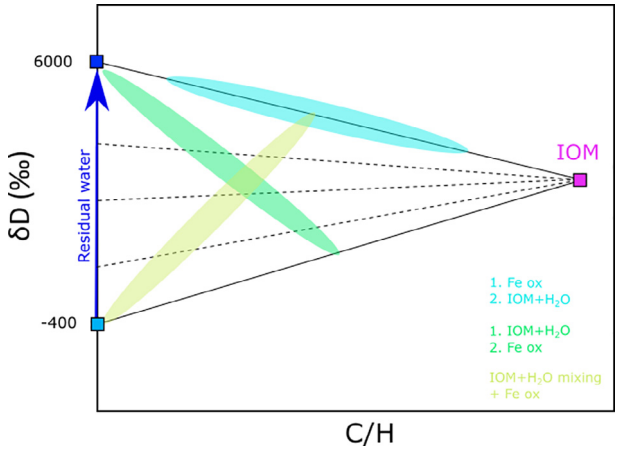

Fig. 15. D/H versus C/H plot demonstrating different scenarios for CM chondrite alteration, with various sequences of Fe oxidation and mixing between water and D-rich organic matter. The maximal residual water D/H ratio is taken from Sutton et al. (2017) and the IOM composition is from Alexander et al. (2012).

4.2.2. H_2 release during serpentinization

Similar to oxidation of Fe metal, serpenitization of ferromagnesian silicates during hydrothermal alteration (e.g., hydroxylation) is known to release significant amounts of H_2 gas and should therefore be considered as a potential mechanism to increase D/H ratios of serpentine-rich chondrite matrix. H_2 release by serpentinization is not limited by low abundances of precursor materials, unlike the previously mentioned Fe oxidation process. The production of H_2 during serpenitization is dependent on many factors, including the Fe/Mg ratio of the precursor silicates, the thermodynamic conditions of the reaction, the efficiency of H_2 removal and the fluid flow rate among others (Holm et al., 2015). The initial Fe/Mg ratio of matrix silicates is important, since it determines how much H_2 will be produced accordingly (Oze and Sharma, 2007):

$$\mathbf{Fo_{100}}: 2Mg_2SiO_4 + 3H_2O \rightleftharpoons Mg_3Si_2O_5(OH)_4 + Mg(OH)_2 \quad (2)$$

$$\mathbf{Fo_{50}}: 3FeMgSiO_4 + 3H_2O \rightleftharpoons Mg_3Si_2O_5(OH)_4 + SiO_2 + Fe_3O_4 + H_2 \quad (3)$$

where Fo depicts the forsterite content of the initial olivine composition. These reactions show that more H_2 is produced with a higher Fe content in olivine. However, a caveat here is that, thermodynamically speaking, serpenitization of Fe-rich olivine is not a favourable reaction (at $<Fo_{50}$ and variable P-T conditions, olivine is consumed rather than produced) and when reaction 3 reaches equilibrium H_2 will be consumed again in a backward reaction to form anhydrous silicates (Oze and Sharma, 2007). Hence, in order to have a significant H_2 production, abundant Fe-rich silicates and efficient removal of the gas are required (Holm et al., 2015). The least altered CR3 and CO3 chondrites show high modal abundances of Fe-rich amorphous silicates

(CR: <15 vol%, Howard et al., 2011; CO: 23–37 vol%, Howard et al., 2014), indicating that the initial conditions for H_2 production by serpentinization would have been optimal. However, it is unclear whether hydration of amorphous silicates produces a similar amount of H_2 as the serpentinization reaction of Fe-rich olivine and if CM chondrites accreted similar amounts of Fe-rich silicates as CR chondrites. Furthermore, during the onset of aqueous alteration, the first minerals to be transformed besides amorphous silicates are Fe-rich fine-grained olivines or pyroxenes, after which the more Mg-rich minerals react to form oxidized secondary phases (Zolensky et al., 1993; Browning et al., 1996; Leroux et al., 2015; King et al., 2017). Consequently and contrary to our observations, reactions 2 and 3 show that progressive serpentinization leads to increasingly D-poor phyllosilicates in more altered CM chondrites. Moreover, oxygen isotope signatures from calcite grains in CM chondrites predict a closed system for a more or less static fluid (Lindgren et al., 2017), in agreement with the low permeability of CM chondrites (Bland et al., 2009) and compositional indicators of a static fluid from olivine replacement by serpentine (Velbel et al., 2012). These findings suggest that H_2 removal was not very efficient, reducing the likelyhood of significant D/H fractionation during serpentinization. Contrary to these findings, Pignatelli et al. (2017) suggest that H_2 degassing by serpentinization on the CM chondrite parent body was a likely occurrence, based on high Fe^{3+}/Fe_{total} ratios in TCIs from the Paris meteorite. These values do imply highly oxidizing conditions during aqueous alteration, which, however, could also be explained by high water/rock ratios. Nevertheless, we would expect an increasing Fe^{3+}/Fe_{total} with progressive serpentinization, a trend that is not readily observed from increasingly altered CM chondrites.

4.2.3. Decomposition of TCIs

We propose an alternative mechanism to increase the D/H ratio of phyllosilicates in the matrix during progressive aqueous alteration of CM chondrites. The initial mineralogy of chondrite matrices mainly consists of anhydrous silicates (crystalline olivine and pyroxene and amorphous ferromagnesian silicates) and FeNi metal (Abreu and Brearley, 2010; LeGuillou et al., 2015). During the onset of aqueous alteration, the first secondary phases in CM chondrites are tochilinite and cronstedtite (Pignatelli et al., 2017), either as intergrowths (TCIs) or as separate phases (e.g., Maribo, Fig. 16.1) according to the following generalized reaction that includes FeNi metal reacting with either Fe-rich or Mg-rich olivine:

$$\underset{\text{metal}}{\text{FeNi}} + \underset{\text{olivine}}{(\text{Fe},\text{Mg})_2\text{SiO}_4} + \text{H}_2\text{O} \rightleftharpoons \underset{\text{tochilinite}}{6\text{FeS}\cdot 5[(\text{Mg},\text{Fe})(\text{OH})_2]} + \underset{\text{cronstedtite}}{\text{Fe}_{e_2}{}^{2+}\text{Fe}^{3+}(\text{Si},\text{Fe}^{3+})\text{O}_5(\text{OH})_4} \quad (4)$$

The H isotope signature of these first formed TCIs would lie on a mixing line between D-rich organic matter and D-poor water, depending when and to which extent the water is exchanging with the organic matter. With increasing amounts of water altering the matrix, relative to the abundance of organic matter, we expect the D/H ratio of matrix phyllosilicates to decrease as indicated by the D/H ratios of variably altered regions of Paris (Piani et al., 2018). The C/H ratio will also decrease, since H is increasing at a higher rate than the C from a CO_2-rich fluid that will produce carbonates. This first phase of alteration is expected to continue until either FeNi metal or anhydrous silicates are consumed (Fig. 16.2). Maribo and the more altered regions of Paris have few anhydrous silicate grains in their matrix (this work and Hewins et al., 2014), indicating that almost all anhydrous minerals are consumed by phyllosilicates. Since these CM chondrites are assigned petrological type 2.7 or higher, we suggest that Paris and Maribo represent the final stages of the first phase of alteration. During the second phase (Fig. 16.3), progressive alteration at higher temperatures converts tochilinite in TCIs to coarser FeS grains ($T > 245$ °C, Fuchs et al., 1973) and cronstedtite to more Mg-rich phyllosilicates such as chrysotile (Rubin et al., 2007), such that the overall reaction is:

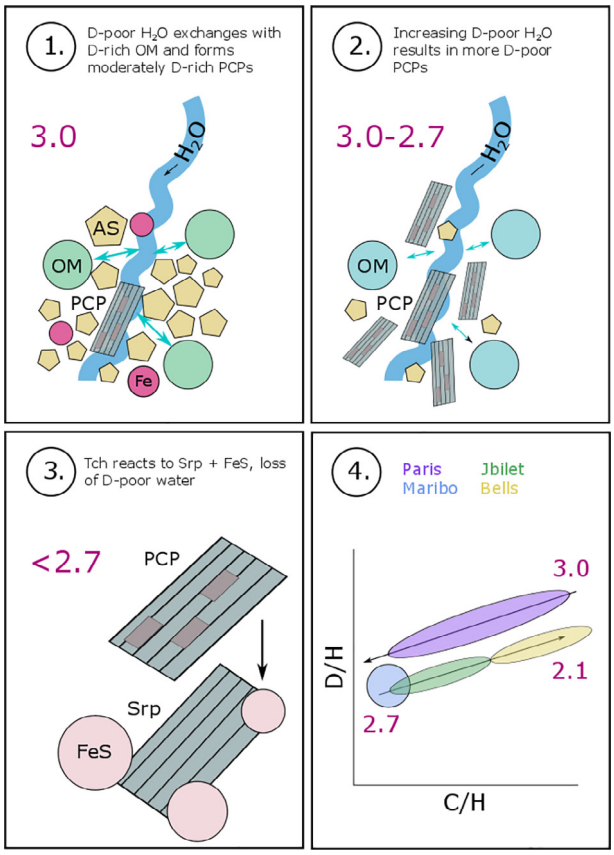

Fig. 16. Hypothetical scenario for CM chondrite alteration explaining mineralogy and H isotope signatures. (1 and 2) First stage of aqueous alteration from type 3.0 to ~2.7, where D-rich organic matter (OM) is oxidized by increasing amounts of D-poor water forming PCP structures from Fe metal (Fe) and anhydrous silicates (AS). (3) Second stage of alteration, where PCP structures are decomposed to iron sulfides (FeS) and Mg-rich serpentines (Srp), resulting in the release of D-poor water in gaseous form. (4) Overview of alteration scenario for the H isotope composition of CM chondrites.

$$\underset{\text{tochilinite}}{6FeS \cdot 5[(Mg,Fe)(OH)_2]} + 3.33SiO_2(aq) \rightleftharpoons \underset{\text{troilite}}{6FeS} + \underset{\text{Mg-rich serpentine}}{1.67(Mg,Fe)_3Si_2O_5(OH)_4} + 1.67H_2O(g) \quad (5)$$

Recent estimations of peak temperatures for carbonate precipitation in CM chondrites are <300 °C, Verdier-Paoletti et al. (2017). Depending on the redox state of the hydrothermal system, the brucite part of the tochilinite structure can also decompose to serpentine and magnetite (Bach et al., 2006) accordingly:

$$\underset{\text{brucite}}{57[(Mg,Fe)(OH)_2]} + 30SiO_2(aq) \rightleftharpoons \underset{\text{magnetite}}{4Fe_3O_4} + \underset{\text{Mg-rich serpentine}}{15(Mg,Fe)_3Si_2O_5(OH)_4} + 23H_2O(g) + 4H_2(g) \quad (6)$$

Observations of the secondary phases found in the most altered CM chondrites suggest that the abundance of magnetite (2–3 vol%, King et al., 2017) is similar to that of sulfide (<5 vol%, Bach et al., 2006; King et al., 2017). However, most magnetite is situated within chondrules and is associated with metal oxidation. TEM observations of Maribo, Jbilet Winselwan and Bells matrices indicate that the decomposition of TCIs is associated with an increasing abundance of FeS, favouring reaction 5. Consequently, the replacement of tochilinite by FeS and increase of the phyllosilicate/sulfide ratio in TCIs results in a net loss of water, since tochilinite contains ~37 mol% of OH and serpentine ~28 mol%. The decomposition of tochilinite is a forward reaction as indicated by the FeS-rich/Tch-poor mineralogy of highly altered CM chondrites such as Bells. Hence, during this stage of relative dehydration, we suggest the D/H signature of the matrix to increase, as is expected for devolatization reactions on planetary bodies. Collectively, H isotope systematics of CM chondrite matrix are expected to behave differently during progressive aqueous alteration. During the first stage of serpentinization, we expect a decrease of D/H with decreasing C/H, whereas during the second stage of TCI decomposition, we expect the opposite behaviour (Fig. 16.4). The sequence of alteration outlined in Fig. 16 is likely unique to CM chondrites, since these meteorites contain abundant cronstedtite as alteration product relative to other chondrites. This is likely owed to variations in bulk chemical composition due to heterogeneous accretion of chondritic components such as chondrules, matrix, CAIs and ices as well as conditions of alteration on the chondrite parent bodies (LeGuillou et al., 2015). Lastly, we note that the H isotope composition of Jbilet is not homogeneous for both matrix regions analyzed. The clast represented by mx1 is in fact more D-poor than the bulk of the section represented by mx2 (Fig. 14). The matrix in clast mx1 is different from that of mx2 and has more anhydrous silicates, while at the same time having a more altered, saponite-rich mineralogy. This contradictory mineralogy as well as the blotchy texture of the matrix in mx1 from EMP imaging (Fig. 4, mx1) indicates secondary heating after aqueous alteration (Zolensky et al., 2016), which is also suggested from the structure of the organic matter (see Section 4.3.2). This secondary heating may have resulted in loss of H- and C-rich gasses, as implied by Fig. 14, where a relative loss of hydrogen is observed (Fig. 14a).

4.3. Structural changes in organic matter during aqueous and thermal alteration

Maribo is one of two relatively unaltered CM chondrites, the second being Paris with a petrological type of ~2.9. Unlike Paris, Maribo has a homogeneous texture and exhibits a similar low degree of alteration throughout the meteorite, which is assigned petrological type >2.7. The degree of alteration in Maribo is likely similar to Paris, considering its bulk oxygen isotope and PCP composition (Haack et al., 2012), the abundant small metal grains surviving in the matrix, the presence of amorphous and anhydrous silicates and the ubiquitous fine-grained TCI structures. The organic structure of Paris IOM has been determined using multiple techniques, including ^{13}C nuclear magnetic resonance (NMR) spectroscopy, C-XANES and pyrolysis gas chromatography mass spectroscopy (GC-MS) (Vinogradoff et al., 2017). These techniques involve analyses of separated IOM by crushing multiple grams of the Paris meteorite, thereby including fresh and altered regions. NMR and C-XANES results show that Paris contains more or less equal amounts of aromatic/olefinic and aliphatic compounds, with 25% variability in aromatic and carboxylic abundances and 20% variability in ketone/nitrile related structures. Comparing results from pyrolysis GC-MS between Paris and Murchison, however, indicates that Paris has a higher relative abundance of aromatics than suggested from NMR spectroscopy. Vinogradoff et al. (2017) also observe an increase in aromatic carbon (>50%), ketones, carboxyls and carbonyls (together 15% of the total carbon) for Murchison relative to Paris.

4.3.1. Progressive aqueous alteration

TEM-EELS is not directly comparable to the methods used for the determination of the Paris organic structure. However, we can characterize changes in the carbon and nitrogen structure during aqueous alteration from Maribo to Jbilet Winselwan and Bells (Fig. 13). First, we observe significant differences in carbon structures between Maribo and Jbilet Winselwan mx2. The carbon functional groups of Jbilet Winselwan mx2 contain an increasing amount of ketone (C═O), aliphatic (C─C) and carboxyl (COOH), relative to aromatic/olefinic and alkene bonding environments (C═C). We rule out the possibility of nitrile contribution at the 286.5 eV peak, since the N-K edge of Jbilet Winselwan mx1 does not show any evidence of nitrile bonding (399–400 eV). These changes likely represent oxidation of organic matter during progressive aqueous alteration (Fig. 17). During this process, we do not expect the nitrogen structure to change, as is evidenced by similarities between N-K edges of Maribo and Jbilet Winselwan mx1. In addition, we observe an increase in the C/N ratio with progressive alteration, suggesting loss of N. The C-K edge structures of Bells are very similar to those of Jbilet Winselwan mx2, albeit with a relatively higher peak at 286.5 eV, suggesting that Bells has experienced a higher degree of alteration. Our results are in agreement with Vinogradoff

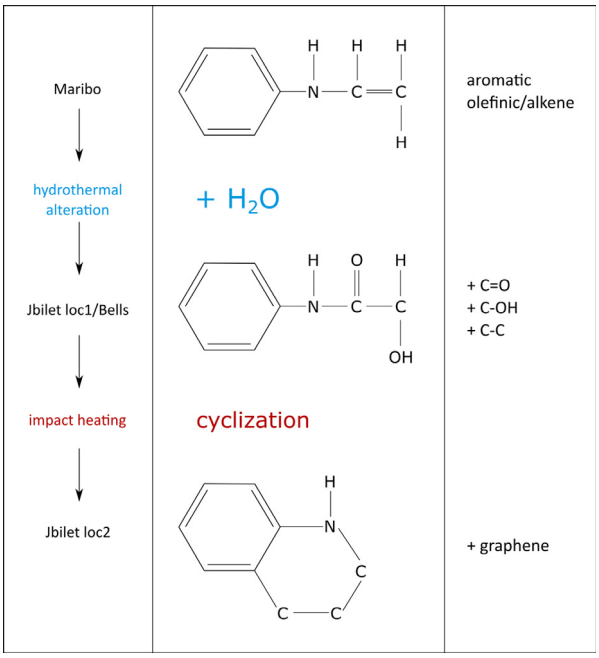

Fig. 17. Schematic overview of changes to the structure of organic matter in CM chondrites during aqueous alteration, as observed from C-K and N-K EELS of Maribo, Jbilet Winselwan and Bells.

et al. (2017), who observe an increase of ketone and carboxyl functional groups between Paris and Murchison. They suggest, however, a higher initial aliphatic/aromatic ratio for Paris IOM and increasing aromatization during aqueous alteration. This contradicts pyrolysis GC-MS and Fourier Transform Mass Spectrometry (FTMS) observations from Maribo, which suggest that Maribo has a higher aromaticity than Murchison (Haack et al., 2012). Similarly, our TEM-EELS results suggest that the aliphatic/aromatic ratio increases with progressive aqueous alteration. Haack et al. (2012) propose that this trend is related to the chemical degradation of organic matter during oxidation reactions according to the following reaction:

$$\underset{\text{alkene}}{CH_2=CH_2} + H_2O \rightleftharpoons \underset{\text{aliphatic}}{CH_3-CH_2OH} \quad (7)$$

During this process double carbon bonds are broken in favour of oxygen and hydroxyl bonding environments (Fig. 17). The apparent differences between Paris and Maribo organic matter may be related to different sample preparation and analytical techniques. Paris IOM was extracted by repeated use of solvents such as water that perhaps oxidize the organic matter. In contrast, Maribo bulk sample was directly heated during pyrolysis GC-MS measurements. Moreover, the Paris sample includes more altered regions, which may express different aliphatic/aromatic ratios. While results from pyrolysis GC-MS and FTMS (Haack et al., 2012) agree with TEM-EELS carbon structures of Maribo versus more altered CM chondrites such as Murchison and Jbilet Winselwan, pyrolysis GC-MS of Paris does not agree well with C-XANES and NMR spectroscopy results of Vinogradoff et al. (2017). This may be related to a low degree of cross-linking between aromatic moieties of Paris IOM, thus rendering the aromatics more thermally labile. Consequently, if differences between Paris and Maribo do not reflect analytical artefacts, these pristine CM chondrites must have accreted IOM with different compositions. We propose that Paris accreted earlier than other CM chondrites and that its IOM is not representative of the CM chondrite parent body. This is in agreement with the old ^{53}Mn-^{53}Cr chondrule age (4566.44 ± 0.66 Ma, Hewins et al., 2014) and perhaps also with the deviating H isotope signatures of Paris. Indeed, while Maribo and other CM chondrites have similar intercepts in D/H versus C/H space (Fig. 14b, Piani et al., 2018), Paris either has a different intercept as suggested by Piani et al. (2018), or arguably a different slope. The latter would suggest that Paris accreted more D-rich organic matter, which is not observed from IOM analyses (Vinogradoff et al., 2017). However, a different intercept indicates accretion of more D-rich water ice, which is favourable for an early accretion model: the water ice, inherited from cold interstellar environments would have had no time to equilibrate with H_2 gas from the protoplanetary disk (Yang et al., 2013). Similarly, shorter residence times of IOM in the disk, may have led to higher aliphatic/aromatic ratios. Consequently, we speculate that Maribo, but not Paris may be representative of precursor material to more altered CM chondrites.

4.3.2. Impact heating

In Section 4.2, we discussed the possibility that the clast represented by Jbilet Winselwan mx1 was affected by a secondary heating event. This interpretation was made based on the mineralogy of the matrix and the H isotope composition of mx1. Between Jbilet Winselwan mx2 and mx1 C-K edges we observe a significant increase of the 291 eV peak, which corresponds to C—C bonds in graphene or polycyclic carbons. In addition, we find smaller changes in the intensities of peaks in the π^* transition, including an increase at 288 eV (CH_n), a decrease at 288.5 (COOH) and at 286.5 (C=O) with a higher intensity of the 291 eV peak. These changes are best explained by cyclization/graphitization of carbon chains during heating of organic matter (Fig. 17). The corresponding temperatures of this process ($T > 750$ °C) are not in range of typical hydrothermal alteration of CM chondrites ($T < 300$ °C; Keil, 2000; Verdier-Paoletti et al., 2017), but are most likely the result of impact heating suggested for some clasts of the Jbilet Winselwan breccia (Zolensky et al., 2016). The lower C/N ratios of Jbilet Winselwan mx1 organic matter, as well as the lower C/H ratios mx1 matrix relative to mx2 are consequently related to loss of carbon, perhaps through CO_2 degassing.

5. CONCLUSIONS

We report on the N, C and H isotope composition as well as the structure of organic matter of CM chondrites showing progressive aqueous alteration. This includes one of the most unaltered CM chondrites, Maribo (type ~2.8), the moderately altered Jbilet Winselwan (type 2.3–2.6) and the highly altered anomalous CM chondrite Bells (type 2.0–2.1). Based on the mineralogy, stable isotope

compositions and structure of the organic matter of CM chondrites, we provide the following constraints on the formation history of CM chondrites:

(1) Maribo's texture includes porphyritic olivine chondrules with iron oxide inclusions, tochilinite and cronstedtite grains surrounded by singular dust rims, which represent the matrix component of Maribo. Jbilet Winselwan looks like a more altered version of Maribo, albeit more brecciated, with multiple rim structures surrounding the chondrules and tochilinite-cronstedtite intergrowths. Bells contains more abundant intra-chondrule matrix with a higher abundance of magnetite and FeNi metal. Its chondrules also contain FeNi metal inclusions instead of iron oxides.

(2) Maribo's fine-grained matrix mineralogy includes abundant tochilinite-cronstedtite intergrowths, aggregates of FeNi metal nuggets surrounded by iron oxide rims and amorphous as well as anhydrous silicates. The more altered Jbilet Winselwan contains coarser FeS grains separated from serpentine laths and often clustered with semi-globular organic matter. Bells also contains FeS grains, magnetite aggregates and individual globular organic matter embedded in a saponite matrix.

(3) N isotope behaviour during alteration is characterized by an increase in ^{15}N-rich hotspots, but a lowering of the magnitude of enrichment in indiviudal hotspot domains, suggesting a homogenization of the N isotope signature throughout the matrix. Bulk δ^{15}N values measured by SIMS likely represent SOM isotope signatures instead of IOM *and* SOM. We suggest that N isotope variations found between bulk CM chondrites in the order of tens of permil are the result of aqueous alteration, whereas variations of hundreds of permil are most likely caused by heterogeneous accretion of IOM and SOM-like components in the protoplanetary disk. Bells is an example of heterogeneous accretion of IOM on the CM chondrite parent body.

(4)] We observe a correlation between progressive aqueous alteration and increasing D/H ratios from matrix of Maribo > Jbilet Winselwan > Bells. This correlation is best explained by decomposition of TCIs, which react to iron sulfides and more Mg-rich serpentine. During this process (petrological type >2.7) water is released and degassed, resulting in more D-rich residual phyllosilicates. The first stage of alteration shows H isotope behaviour in the opposite direction and is likely related to increasing oxidation of D-rich organic matter by D-poor water.

(5) Maribo's organic structure uniformly consists of a higher aromatic/aliphatic ratio relative to Jbilet Winselwan and Bells. In addition, the more altered CM chondrites contain higher abundances of ketone and carboxyl functional groups related to increasing oxidation of organic matter. We suggest that this oxidation process results in the decomposition of aromatic and alkene bonding environments with progressive aqueous alteration. In contrast, the Paris meteorite (type >2.7) contains a lower aromatic/aliphatic ratio than more altered CM chondrites, most likely suggesting that Paris accreted a different type of IOM than Maribo. We propose that Maribo, not Paris, is most representative of precursor material to organic matter in CM chondrites.

ACKNOWLEDGMENTS

This work was funded by grants from the Danish National Research Foundation (DNRF97) and from the European Research Council (ERC Consolidator grant agreement 616027-STARDUST2 ASTEROIDS) to M.B.

APPENDIX A. FE OXIDATION AND H ISOTOPE FRACTIONATION

Fe metal reacts with water according to the following reaction:

$$3Fe + 4H_2O \rightleftharpoons Fe_3O_4 + 4H_2\ (g)$$

If we assume 3 wt% of Fe_{met} and 20 wt% H_2O (Garenne et al., 2014) as initial conditions of the CM chondrite parent body, for every gram of Fe_{met} that reacts to form Fe_3O_4, we need 0.81 gram of H_2O. Consequently, if we consume all Fe_{met} on the CM chondrite parent body, 12.2% of the total water budget is consumed during oxidation. We note that these initial conditions are very conservative estimates, since the amount of metal in Paris may be anomalous compared to the much lower amount of metal observed in Maribo. Furthermore, the initial water/rock ratio in CM chondrites may be much higher. The weight percentage used here is derived from phyllosilicate stoichiometry.

If we use equilibrium fractionation of H_2O-H_2, we can calculate the D/H ratio of the residual water with the initial $D/H = 1.00 \times 10^{-4}$, the residual fraction of water f is 0.88 and the fractionation factor α is from Suess (1949):

$$1000 ln\alpha = \frac{467600}{T} - 303.9 \quad (2)$$

where T is the temperature in Kelvin. If we use an average temperature for hydrothermal alteration of 373 K (Brearley, 2006), then the maximum D/H ratio that the most altered CM chondrites could achieve is:

$$\frac{D}{H} = \frac{D}{H_0} \times f^{\frac{1}{\alpha}-1} = 1.08 \times 10^{-4} \quad (3)$$

APPENDIX B. SUPPLEMENTARY MATERIAL

Supplementary data associated with this article can be found, in the online version, at https://doi.org/10.1016/j.gca.2018.06.021.

REFERENCES

Abreu N. M. and Brearley A. J. (2010) Early solar system processes recorded in the matrices of two highly pristine CR3 carbonaceous chondrites, MET 00426 and QUE 99177. *Geochim. Cosmochim. Acta* **74**, 1146–1171.

Aléon J. (2010) Multiple origins of nitrogen isotopic anomalies in meteorites and Comets. *Astrophys. J.* **722**, 1342.

Alexander C. M. O., Fogel M., Yabuta H. and Cody G. D. (2007) The origin and evolution of chondrites recorded in the elemental and isotopic compositions of their macromolecular organic matter. *Geochim. Cosmochim. Acta* **71**, 4380–4403.

Alexander C. M. O., Bowden R., Fogel M. L., Howard K. T., Herd C. D. K. and Nittler L. R. (2012) The provenances of asteroids, and their contributions to the volatile inventories of the terrestrial planets. *Science* **337**, 721–723.

Alexander C. M. O., Howard K. T., Bowden R. and Fogel M. L. (2013) The classification of CM and CR chondrites using bulk H, C and N abundances and isotopic compositions. *Geochim. Cosmochim. Acta* **123**, 244–260.

Alexander C. M. O., Bowden R., Fogel M. L. and Howard K. T. (2015) Carbonate abundances and isotopic compositions in chondrites. *Meteorit. Planet. Sci.* **50**, 810–833.

Alt J. and Shanks W. C. (2015) Stable isotope compositions of serpentinite seamounts in the mariana forearc: serpentinization processes, fluid sources and sulfur metasomatism. *Earth Planet. Sci. Lett.* **242**, 272–285.

Bach W., Paulick H., Garrido C. J., Ildefonse B., Meurer W. P. and Humphris S. E. (2006) Unraveling the sequence of serpentinization reactions: petrography, mineral chemistry, and petrophysics of serpentinites from MAR 15°N (ODP Leg 209, Site 1274). *Geophys. Res. Lett.* **33**, L13306.

Becker R. H. and Epstein S. (1982) Carbon, hydrogen and nitrogen isotopes in solvent-extractable organic matter from carbonaceous chondrites. *Geochim. Cosmochim. Acta* **46**, 97–103.

Bischoff A., Ebert S., Metzler K. and Lentfort S. (2017) Breccia classification of CM chondrites. In *80th Ann. Meet. Met. Soc.*.

Bland P. A., Jackson M. D., Coker R. F., Cohen B. A., Webber J. B. W., Lee M. R., Duffy C. M., Chater R. J., Ardakani M. G., McPhail D. S., McComb D. W. and Benedix G. K. (2009) Why aqueous alteration in asteroids was isochemical: high porosity ¬ = high permeability. *Earth Planet. Sci. Lett.* **287**, 559–568.

Bonal L., Huss G. R., Krot A. N., Nagashima K., Ishii H. A. and Bradley J. P. (2010) Highly ^{15}N-enriched chondritic clasts in the CB/CH-like meteorite Isheyevo. *Geochim. Cosmochim. Acta* **74**, 6590–6609.

Brearley A. J. (1993) Matrix and fine-grained rims in the unequilibrated CO3 chondrite, ALHA77307 – origins and evidence for diverse, primitive nebular dust components. *Geochim. Cosmochim. Acta* **57**, 1521–1550.

Brearley A. J. (1995) Aqueous alteration and brecciation in Bells, an unusual, saponite-bearing, CM chondrite. *Geochim. Cosmochim. Acta* **59**, 2291–2317.

Brearley A. J. (2006) The action of water. In *Meteorites and the Early Solar System II* (eds. D. S. Lauretta and H. Y. McSween Jr.). University of Arizona Press, pp. 584–624.

Browning L. B., McSween H. Y. and Zolensky M. E. (1996) Correlated alteration effects in CM carbonaceous chondrites. *Geochim. Cosmochim. Acta* **60**, 2621–2633.

Budde G., Burkhardt C., Brennecka G. A., Fischer-Gödde M., Kruijer T. S. and Kleine T. (2016) Molybdenum isotopic evidence for the origin of chondrules and a distinct genetic heritage of carbonaceous and non-carbonaceous meteorites. *Earth Planet. Sci. Lett.* **454**, 293–303.

Bunch T. and Chang S. (1980) Carbonaceous chondrites. II – carbonaceous chondrite phyllosilicates and light element geochemistry as indicators of parent body processes and surface conditions. *Geochim. Cosmochim. Acta* **44**, 1543–1577.

Chizmadia L. J. and Brearley A. J. (2008) Mineralogy, aqueous alteration, and primitive textural characteristics of fine-grained rims in the Y-791198 CM2 carbonaceous chondrite: TEM observations and comparison to ALHA81002. *Geochim. Cosmochim. Acta* **72**, 602–625.

Clayton R. N. and Mayeda T. K. (1999) Oxygen isotope studies of carbonaceous chondrites. *Geochim. Cosmochim. Acta* **63**, 2089–2104.

Coakley K. J., Simons D. S. and Leifer A. M. (2005) Secondary ion mass spectrometry measurements of isotopic ratios: correction for time varying count rate. *Int. J. Mass Spec.* **240**, 107–120.

Cody G. and Alexander C. (2005) NMR studies of chemical structural variation of insoluble organic matter from different carbonaceous chondrite groups. *Geochim. Cosmochim. Acta* **69**, 1085–1097.

Cody G. D., Ade H., Alexander C. M. O., Araki T., Butterworth A., Fleckenstein H., Flynn G., Gilles M. K., Jacobsen C., Kilcoyne A. L. D., Messenger K., Sandford S. A., Tyliszczak T., Westphal A. J., Wirick S. and Yabuta H. (2008) Quantitative organic and light-element analysis of comet 81P/Wild 2 particles using C-, N-, and O-μ-XANES. *Meteor. Planet. Sci. Arch.* **43**, 353–365.

Corrigan C. M., Zolensky M. E., Dahl J., Long M., Weir J., Sapp C. and Burkett P. J. (1997) The porosity and permeability of chondritic meteorites and interplanetary dust particles. *Met. Planet. Sci.*, 32.

Cronin J. R. and Chang S. (1993) Organic matter in meteorites: molecular and isotopic analyses of the murchison meteorite. In *In Chemistry of life's origins* (eds. J. M. Greenburg and V. Pirronello). Kluwer, Dordrecht, the Netherlands, pp. 209–258.

De Gregorio B. T., Stroud R. M., Nittler L. R., Alexander C. M. O., Bassim N. D., Cody G. D., Kilcoyne A. L. D., Sandford S. A., Milam S. N., Nuevo M. and Zega T. J. (2013) Isotopic and chemical variation of organic nanoglobules in primitive meteorites. *Meteorit. Planet. Sci.* **48**, 904–928.

Deloule E. and Robert F. (1995) Interstellar water in meteorites? *Geochim. Cosmochim. Acta* **59**, 4695–4706.

Derenne S. and Robert F. (2010) Model of molecular structure of the insoluble organic matter isolated from Murchison meteorite. *Met. Planet. Sci.* **45**, 1461–1475.

Elsila J. E., Charnley S. B., Burton A. S., Glavin D. P. and Dworkin J. P. (2012) Compound-specific carbon, nitrogen, and hydrogen isotopic ratios for amino acids in CM and CR chondrites and their use in evaluating potential formation pathways. *Meteor. Planet. Sci.* **47**, 1517–1536.

Franke R., Bender S. and Hormes J. (1995) N K-shell absorption spectra of ionic and molecular crystals. *Physica B Condens. Matter* **208**, 293–294.

Fuchs L. H., Olsen E. and Jensen K. J. (1973) Mineralogy Mineral-Chemistry and Composition of the Murchison (C2) Meteorite. *Smithsonian Contributions to the Earth Sciences* **10**, 1–39.

Garenne A., Beck P., Montes-Hernandez G., Chiriac R., Toche F., Quirico E., Bonal L. and Schmitt B. (2014) The abundance and stability of "water" in type 1 and 2 carbonaceous chondrites (CI, CM and CR). *Geochim. Cosmochim. Acta* **137**, 93–112.

Grady M. M., Abernethy F. A. J., Verchovsky A. B., King A. J., Schofield P. F. and Russell S. S. (2014) The Jbilet Winselwan carbonaceous chondrite 2. Light element geochemistry strengthening the link between CM and CO meteorites? In *77th Ann. Met. Sco. Meet.*.

Haack H., Grau T., Bischoff A., Horstmann M., Wasson J., Sørensen A., Laubenstein M., Ott U., Palme H., Gellissen M., Greenwood R. C., Pearson V. K., Franchi I. A., Gabelica Z. and Schmitt-Kopplin P. (2012) Maribo—a new CM fall from Denmark. *Meteorit. Planet. Sci.* **47**, 30–50.

Hewins R. H., Bourot-Denise M., Zanda B., Leroux H., Barrat J.-A., Humayun M., Göpel C., Greenwood R. C., Franchi I. A., Pont S., Lorand J.-P., Cournède C., Gattacceca J., Rochette P., Kuga M., Marrocchi Y. and Marty B. (2014) The Paris

meteorite, the least altered CM chondrite so far. *Geochim. Cosmochim. Acta* **124**, 190–222.
Holm N. G., Oze C., Mousis O., Waite J. H. and Guilbert-Lepoutre A. (2015) Serpentinization and the formation of H2 and CH4 on celestial bodies (Planets, Moons, Comets). *Astrobiology* **15**, 587.
Howard K. T., Benedix G. K., Bland P. A. and Cressey G. (2009) Modal mineralogy of CM2 chondrites by X-ray diffraction (PSD-XRD). Part 1: Total phyllosilicate abundance and the degree of aqueous alteration. *Geochim. Cosmochim. Acta* **73**, 4576–4589.
Howard K. T., Benedix G. K., Bland P. A. and Cressey G. (2011) Modal mineralogy of CM chondrites by X-ray diffraction (PSD-XRD): Part 2. Degree, nature and settings of aqueous alteration. *Geochim. Cosmochim. Acta* **75**, 2735–2751.
Howard K., Alexander C. and Dyl K. (2014) PSD-XRD modal mineralogy of type 3.0 CO chondrites: initial asteroidal water mass fractions and implications for CM chondrites. In *Lun. Planet. Sci. Con.*, p. 1830.
Kallemeyn G. W. (1995) Bells and Essebi: to be or not to be (CM). *Meteoritics*, 30.
Keil K. (2000) Thermal alteration of asteroids: evidence from meteorites. *Planet. Space Sci.* **48**, 887–903.
King A. J., Schofield P. F. and Russell S. S. (2017) Type 1 aqueous alteration in CM carbonaceous chondrites: implications for the evolution of water-rich asteroids. *Meteorit. Planet. Sci.* **52**, 1197–1215.
Krot A., Keil K., Goodrich C. and Scott E. (2003) Classification of meteorites. In *Meteorites, Comets, and Planets, Treatise on Geochemistry*, vol. 1 (ed. A. M. Davis). Elsevier-Pergamon, Oxford, pp. 83–127.
Lajaunie L., Boucher F., Dessapt R. and Moreau P. (2015) Quantitative use of electron energy-loss spectroscopy Mo-M2,3 edges for the study of molybdenum oxides. *Ultramicroscopy* **149**, 1–8.
Lauretta D. S., Hua X. and Buseck P. R. (2000) Mineralogy of fine-grained rims in the ALH 81002 CM chondrite. *Geochim. Cosmochim. Acta* **64**, 3263–3273.
LeGuillou C., Bernard S., Brearley A. J. and Remusat L. (2014) Evolution of organic matter in Orgueil, Murchison and Renazzo during parent body aqueous alteration: In situ investigations. *Geochim. Cosmochim. Acta* **131**, 368–392.
LeGuillou C., Changela H. and Brearley A. (2015) Widespread oxidized and hydrated amorphous silicates in CR chondrites matrices: implications for alteration conditions and H_2-degassing of asteroids. *Earth Planet. Sci. Lett.* **420**, 162–173.
Leroux H., Cuvillier P., Zanda B. and Hewins R. H. (2015) GEMS-like material in the matrix of the Paris meteorite and the early stages of alteration of CM chondrites. *Geochim. Cosmochim. Acta* **170**, 247–265.
Lindgren P., Lee M. R., Starkey N. A. and Franchi I. A. (2017) Fluid evolution in CM carbonaceous chondrites tracked through the oxygen isotopic compositions of carbonates. *Geochim. Cosmochim. Acta* **204**, 240–251.
Messenger S., Nakamura-Messenger K. and Keller L. P. (2008) N-15-Rich Organic Globules in a Cluster IDP and the Bells CM2 Chondrite. In *39th Lun. Planet. Sci. Conf.*.
Mittlefehldt D. W. (2002) Geochemistry of the ungrouped carbonaceous chondrite Tagish Lake, the anomalous CM chondrite Bells, and comparison with CI and CM chondrites. *Meteor. Planet. Sci.* **37**, 703–712.
Monroe A. A. and Pizzarello S. (2011) The soluble organic compounds of the Bells meteorite: not a unique or unusual composition. *Geochim. Cosmochim. Acta* **75**, 7585–7595.
Olsen M. B., Wielandt D., Schiller M., Van Kooten E. M. M. E. and Bizzarro M. (2016) Magnesium and ^{54}Cr isotope compositions of carbonaceous chondrite chondrules – insights into early disk processes. *Geochim. Cosmochim. Acta* **191**, 118–138.
Oze C. and Sharma M. (2007) Serpentinization and the inorganic synthesis of H_2 in planetary surfaces. *Icarus* **186**, 557–561.
Pernet-Fisher J., Howarth G., Barry P., Bodnar R. and Taylor L. (2009) The extent of aqueous alteration within the Jbilet Winselwan CM2 chondrite. In *45th Lun. Planet. Sci. Con.*.
Piani L., Remusat L. and Robert F. (2012) Determination of the H isotopic composition of individual components in fine-scale mixtures of organic matter and phyllosilicates with the nanoscale secondary ion mass spectrometry. *Anal. Chem.* **84**, 10199–10206.
Piani L., Yurimoto H. and Remusat L. (2018) A Dual Origin for Water in carbonaceous chondrites revealed by CM chondrites. *Nat. Astronomy* **2**, 317–323.
Pignatelli I., Marrocchi Y., Mugnaioli E., Bourdelle F. and Gounelle M. (2017) Mineralogical, crystallographic and redox features of the earliest stages of fluid alteration in CM chondrites. *Geochim. Cosmochim. Acta* **209**, 106–122.
Pizzarello S., Cooper G. W. and Flynn G. J. (2006) The nature and distribution of the organic material in carbonaceous chondrites and interplanetary dust particles (eds. D. S. Lauretta and H. Y. McSween Jr.). University of Arizona Press, Tucson, pp. 625–651.
Rowe M. W., Clayton R. N. and Mayeda T. K. (1994) Oxygen isotopes in separated components of CI and CM meteorites. *Geochim. Cosmochim. Acta* **58**, 5341–5347.
Rubin A. E., Trigo-Rodríguez J. M., Huber H. and Wasson J. T. (2007) Progressive aqueous alteration of CM carbonaceous chondrites. *Geochim. Cosmochim. Acta* **71**, 2361–2382.
Russell, S. S., King, A. J., Schofield, P. F., Verchovsky, A. B., Abernethy, F. A. J., and Grady, M. M. (2014). The Jbilet Winselwan Carbonaceous Chondrite 1 Mineralogy and Petrology: Strengthening the Link Between CM and CO Meteorites? 77th Annual Meeting of the Meteoritical Society, held September 7-12, 2014 in Casablanca, Morocco. LPI Contribution No. 1800. pp. 5253.
Scott E. (2007) Chondrites and the protoplanetary disk. *Annu. Rev. Earth Planet. Sci.* **35**, 577–620.
Suess H. (1949) Das Gleichgewicht $H_2 + HDO = HD + H_2O$ und die weiteren Austauschgleichgewichte im System H_2, D_2 und H_2O. *Z. Naturforsch. A* **4**.
Sutton S., Alexander C. M. O., Bryant A., Lanzirotti A., Newville M. and Cloutis E. A. (2017) The bulk valence state of Fe and the origin of water in chondrites. *Geochim. Cosmochim. Acta* **211**, 115–132.
Tomeoka K. and Buseck P. R. (1985) Indicators of aqueous alteration in CM carbonaceous chondrites: Microtextures of a layered mineral containing Fe, S, O and Ni. *Geochim. Cosmochim. Acta* **49**, 2149–2163.
Tomeoka K. and Buseck P. R. (1988) Matrix mineralogy of the Orgueil CI carbonaceous chondrite. *Geochim. Cosmochim. Acta* **52**, 1627–1640.
Tomeoka K., McSween, Jr., H. Y. and Buseck P. R. (1989) Mineralogical alteration of cm carbonaceous chondrites: a review. *Antarct. Meteor. Res.*, 221.
Vacher L. G., Marrocchi Y., Verdier-Paoletti M. J., Villeneuve J. and Gounelle M. (2016) Inward radial mixing of interstellar water ices in the solar protoplanetary disk. *Astrophys. J. Lett.* **827**, L1.
Van Kooten E. M. M. E., Wielandt D., Schiller M., Nagashima K., Thomen A., Larsen K. K., Olsen M. B., Nordlund Å., Krot A. N. and Bizzarro M. (2016) Isotopic evidence for primordial molecular cloud material in metal-rich carbonaceous chondrites. *Proc. Nat. Ac. Sci., USA* **113**, 2011–2016.

van Kooten E. M. M. E., Nagashima K., Kasama T., Wampfler S. F., Ramsey J. P., Frimann S., Balogh Z. I., Schiller M., Wielandt D. P., Franchi I. A., Jørgensen J. K., Krot A. N. and Bizzarro M. (2017) A divergent heritage for complex organics in Isheyevo lithic clasts. *Geochim. Cosmochim. Acta* **205**, 119–148.

Velbel M. A., Tonui E. K. and Zolensky M. E. (2012) Replacement of olivine by serpentine in the carbonaceous chondrite Nogoya (CM2). *Geochim. Cosmochim. Acta* **87**, 117–135.

Verdier-Paoletti M., Marrocchi Y., Avice G., Roskosz M., Gurenko A. and Gounelle M. (2017) Oxygen isotope constraints on the alteration temperatures of CM chondrites. *Earth Planet. Sci. Lett.* **458**, 273–281.

Vinogradoff V., Le Guillou C., Bernard S., Binet L., Cartigny P., Brearley A. J. and Remusat L. (2017) Paris vs. Murchison: Impact of hydrothermal alteration on organic matter in CM chondrites. Geochim. Cosmochim. *Acta* **212**, 234–252.

Vollmer C., Barth M., Le Guillou C., Ramasse Q. M., Horstmann M. and Bischoff A. (2014) The early stages of aqueous alteration in CM chondrites – TEM-ULTRASTEM-STXM investigations of the less-altered chondrite Maribo. In *45th Lun. Planet. Sci. Con.*.

Weisberg M. K., Prinz M., Clayton R. N. and Mayeda T. K. (1993) The CR (Renazzo-type) carbonaceous chondrite group and its implications. *Geochim. Cosmochim. Acta* **57**, 1567–1586.

Wiliford K., Ushikubo T., Lepot K., Kitajima K., Hallmann C., Spicuzza M., Kozdon R., Eigenbrode J., Summons R. and Valley (2016) Carbon and sulfur isotopic signatures of ancient life and environment at the microbial scale: neoarchean shales and carbonates. *Geobiology* **14**, 105–128.

Yang L., Ciesla F. J. and Alexander C. M. O. (2013) The D/H ratio of water in the solar nebula during its formation and evolution. *Icarus* **226**, 256–267.

Zadnik M. (1985) Noble gases in the bells (C2) and sharps (H3) chondrites. *Meteoritics* **20**, 245–257.

Zanda B., Bourot-Denise M., Hewins R., Barrat J. and Gattacceca J. (2010) The Paris CM chondrite yields new insights on the onset of parent body alteration. *Meteorit. Planet. Sci.*, 45.

Zolensky M., Barrett R. and Burkett P. J. (1993) Chondritic interplanetary dust particles: mineral compositions and petrofabrics. *Meteoritics*, 28.

Zolensky M. E., Weisberg M. K., Buchanan P. C. and Mittlefehldt D. W. (1996) Mineralogy of carbonaceous chondrite clasts in HED achondrites and the Moon. *Meteor. Planet. Sci.* **31**, 518–537.

Zolensky M. E., Mikouchi T., Hagiya K., Ohsumi K., Komatsu M., Chan Q., Le L., Kring D., Cato M., Fagan A., Gross J., Tanaka A., Takegawa D., Hoshikawa T., Yoshida T. and Sawa N. (2016) Unique view of C asteroid regolith from the Jbilet Winselwan CM chondrite. In *47th Lun. Planet. Sci. Con.*.

Associate editor: Sara S. Russell